

HYBRIDIZED DISCONTINUOUS GALERKIN METHODS FOR A MULTIPLE NETWORK POROELASTICITY MODEL WITH MEDICAL APPLICATIONS

JOHANNES KRAUS, PHILIP L. LEDERER, MARIA LYMBERY, KEVIN OSTHUES,
AND JOACHIM SCHÖBERL

ABSTRACT. The quasi-static multiple network poroelastic theory (MPET) model, first introduced in the context of geomechanics, has recently found new applications in medicine. In practice, the parameters in the MPET equations can vary over several orders of magnitude which makes their stable discretization and fast solution a challenging task. Here, a new efficient parameter-robust hybridized discontinuous Galerkin method, which also features fluid mass conservation, is proposed for the MPET model. Its stability analysis which is crucial for the well-posedness of the discrete problem is performed and cost-efficient fast parameter-robust preconditioners are derived. We present a series of numerical computations for a 4-network MPET model of a human brain which support the performance of the new algorithms.

1. INTRODUCTION

According to a United Nations report, [24], the proportion of people in 2020 worldwide older than 65 was 9.3% and is expected to reach 16.0% in 2050. As a result of an ageing population health care services have to put more focus on age related diseases, in particular those affecting the brain, such as dementia and stroke as these have a serious impact on quality of life and consequently healthcare costs. In all this treating brain diseases is rather onerous. Being the most complex organ in the human body and difficult to access and study in situ, the brain remains substantially an enigma and non-destructive approaches are required for the study of its physiology. One such approach is naturally mathematical modeling. A model that has been used to simulate the physiology of neurodegenerative conditions such as brain aneurism is the fluid-structure interaction model, see [10], which consists of a two-fields problem, coupling the incompressible Navier-Stokes equations with the non-linear elastodynamics equation modeling the solid deformation. In this paper we consider the Multiple-network PoroElastic Theory (MPET) model that has been widely used to investigate blood and tissue fluid flow interactions in the human brain and related brain pathologies such as Alzheimer’s disease, [11], acute hydrocephalus, [3, 27], ischaemic stroke, [12].

The MPET model equations in a bounded domain $\Omega \subset \mathbb{R}^d$, $d = 1, 2, 3$ encompassing n fluid networks, for $i = 1, \dots, n$ are given as:

$$(1a) \quad -\operatorname{div}(\boldsymbol{\sigma}(\mathbf{u}) - \boldsymbol{\alpha} \cdot p \mathbf{I}) = \tilde{\mathbf{f}}, \quad \text{in } \Omega \times (0, T),$$

$$(1b) \quad K_i^{-1} \mathbf{w}_i + \nabla p_i = \mathbf{0}, \quad \text{in } \Omega \times (0, T),$$

$$(1c) \quad \frac{\partial}{\partial t}(s_i p_i + \alpha_i \operatorname{div} \mathbf{u}) + \operatorname{div} \mathbf{w}_i + \sum_{\substack{j=1 \\ j \neq i}}^n \xi_{ij}(p_i - p_j) = \tilde{g}_i, \quad \text{in } \Omega \times (0, T).$$

Key words and phrases. MPET model, strongly mass-conserving high-order discretizations, parameter-robust LBB stability, norm-equivalent preconditioners, hybrid discontinuous Galerkin methods, hybrid mixed methods.

JK, ML and KO acknowledge the funding by the German Science Fund (DFG) - project “Physics-oriented solvers for multicompartamental poromechanics” under grant number 456235063.

JS acknowledges the funding by the Austrian Science Fund (FWF) through the research programm “Taming complexity in partial differential systems” (F65) - project “Automated discretization in multiphysics” (P10).

PL acknowledges the support by the Academy of Finland (Decision 324611).

The unknown physical quantities in (1) are the tissue deformation $\mathbf{u} = \mathbf{u}(\mathbf{x}, t)$, the network fluid pressures $p_i = p_i(\mathbf{x}, t)$ and respective fluxes $\mathbf{w}_i = \mathbf{w}_i(\mathbf{x}, t)$, $i = 1, \dots, n$. In (1a) we have used the vector notations $\mathbf{p} = (p_1, \dots, p_n)$ and $\boldsymbol{\alpha} = (\alpha_1, \dots, \alpha_n)$ with $\alpha_i \in (0, 1]$ denoting the Biot-Willis constant for the i -th network. The elastic stress tensor in (1a) is defined as

$$\boldsymbol{\sigma}(\mathbf{u}) = 2\tilde{\mu}\boldsymbol{\epsilon}(\mathbf{u}) + \tilde{\lambda}\operatorname{div}(\mathbf{u})\mathbf{I},$$

where $\boldsymbol{\epsilon}(\mathbf{u}) := (\nabla\mathbf{u} + (\nabla\mathbf{u})^T)/2$ denotes the elastic strain tensor and $\tilde{\lambda}$ and $\tilde{\mu}$ are the Lamé parameters, whereas $\tilde{\mathbf{f}}$ represents a body force density. In (1b) the tensor K_i represents the hydraulic conductivity for the i -th network. The constrained specific storage coefficients are designated by $s_i \geq 0$ in (1c) while \tilde{g}_i are fluid sources. The coupling of two networks i and j is expressed via the network transfer coefficient $\xi_{ij} \geq 0$ for which $\xi_{ij} = \xi_{ji}$ holds.

Solving numerically the MPET system of partial differential equations (1) is an arduous task since the various material parameters involved make it difficult to construct structure-preserving discretizations that are robust and stable in all parameter regimes. Only recently have there been some valuable results in this direction. In [20] a mixed finite element formulation based on introducing a total pressure variable has been shown to be robust for nearly incompressible material, small storage coefficients, and small or vanishing transfer coefficients between networks. A stability analysis of the MPET model (1) that is fully parameter robust along with parameter-robust norm-equivalent preconditioners has been presented in [13]. The latter employs discontinuous Galerkin (DG) schemes to achieve strong mass-conservation.

A major drawback of these schemes, however, remains the high number of globally coupled degrees of freedom that arise in the discrete algebraic system and which consequently makes the construction of efficient fast solvers and preconditioners difficult. An approach to overcome this is hybridization, a process in which continuity constraints of finite element spaces are removed without altering the solution, cf. [4, 5, 6]. This allows the construction of methods that take strengths from both continuous Galerkin (CG) and DG methods, see e.g. [7, 18, 16, 17, 1].

In this paper we propose, analyze and numerically test a new efficient parameter-robust hybridized discontinuous Galerkin method for the MPET model. The remainder of the paper consists of four sections. In Section 2 the initial and boundary conditions completing the MPET system are introduced and the weak formulation of the time-discrete model is presented. A new hybridized DG (HDG) hybrid mixed finite element method in space is then proposed in Section 3 and its parameter-robust well-posedness proven in Section 4 which is the main theoretical contribution of this paper. In Section 5 a norm-equivalent preconditioner is proposed and the theoretical results are complemented through a series of numerical simulations for a 4-network MPET model of a human brain.

2. PROBLEM FORMULATION

In this section a time-discrete weak formulation of (1) is delivered. First, the equations are posed and tested in suitable function spaces and integration by parts is applied. More specifically, the time-dependent trial functions $\mathbf{u}(t)$, $\mathbf{w}(t)$, $\mathbf{p}(t)$ and test functions $\mathbf{v}(t)$, $\mathbf{z}(t)$, $\mathbf{q}(t)$ are to be taken from Hilbert spaces \mathbf{U} , \mathbf{W} , \mathbf{P} which obey essential homogeneous boundary conditions. For the sake of simplicity, the analysis in Section 4 is presented for the case of homogeneous Dirichlet boundary conditions for \mathbf{u} and homogeneous Neumann conditions for the pressures p_i , i.e., homogeneous Dirichlet conditions for the fluxes \mathbf{w}_i . In this situation $\mathbf{U} = \mathbf{H}_0^1(\Omega)$, $\mathbf{W}_i = \mathbf{H}_0(\operatorname{div}, \Omega)$ and $P_i = L_0^2(\Omega)$, $i = 1, \dots, n$. For short, we write $\mathbf{w}^T = (\mathbf{w}_1^T, \dots, \mathbf{w}_n^T)$, $\mathbf{p}^T = (p_1, \dots, p_n)$, $\mathbf{z}^T = (z_1^T, \dots, z_n^T)$, $\mathbf{q}^T = (q_1, \dots, q_n)$ and also $\mathbf{W} = \mathbf{W}_1 \times \dots \times \mathbf{W}_n$, $\mathbf{P} = P_1 \times \dots \times P_n$ and the resulting variational problem reads: For $t \in (0, T)$ and any $(\mathbf{v}, \mathbf{z}, \mathbf{q}) \in \mathbf{U} \times \mathbf{W} \times \mathbf{P}$ find $(\mathbf{u}(t), \mathbf{w}(t), \mathbf{p}(t)) \in \mathbf{U} \times \mathbf{W} \times \mathbf{P}$

such that

$$(2a) \quad \tilde{a}(\mathbf{u}, \mathbf{v}) - \sum_{i=1}^n (\alpha_i p_i, \operatorname{div} \mathbf{v}) = (\tilde{\mathbf{f}}, \mathbf{v}),$$

$$(2b) \quad (K_i^{-1} \mathbf{w}_i, \mathbf{z}_i) - (p_i, \operatorname{div} \mathbf{z}_i) = 0, \quad i = 1, \dots, n,$$

$$(2c) \quad -(\alpha_i \operatorname{div} \partial_t \mathbf{u}, q_i) - (\operatorname{div} \mathbf{w}_i, q_i) - (s_i \partial_t p_i, q_i) - \left(\sum_{\substack{j=1 \\ j \neq i}}^n \xi_{ij} (p_i - p_j), q_i \right) = -(\tilde{g}_i, q_i), \quad i = 1, \dots, n,$$

where

$$(3) \quad \tilde{a}(\mathbf{u}, \mathbf{v}) := 2\tilde{\mu} \int_{\Omega} \boldsymbol{\epsilon}(\mathbf{u}) : \boldsymbol{\epsilon}(\mathbf{v}) \, dx + \tilde{\lambda} \int_{\Omega} \operatorname{div} \mathbf{u} \operatorname{div} \mathbf{v} \, dx.$$

Other scenarios of boundary conditions in general lead to modifications of (2) and in certain cases changes in the parameter-dependent norms involved in the stability analysis may be required, see [15]. The well-posedness of the time-continuous problem then is guaranteed under the initial conditions for \mathbf{u} and \mathbf{p} , i.e., $\mathbf{u}(\cdot, 0) = \mathbf{u}_0(\cdot)$ and $p_i(\cdot, 0) = p_{i,0}(\cdot)$ for $i = 1, \dots, n$.

Next, we use the implicit Euler method to discretize (2) in time obtaining the time-step variational problem: Find $(\mathbf{u}^k, \mathbf{w}^k, \mathbf{p}^k) := (\mathbf{u}(\mathbf{x}, t_k), \mathbf{w}(\mathbf{x}, t_k), \mathbf{p}(\mathbf{x}, t_k)) \in \mathbf{U} \times \mathbf{W} \times \mathbf{P}$ solving the system of equations

$$(4a) \quad \tilde{a}(\mathbf{u}^k, \mathbf{v}) - \sum_{i=1}^n (\alpha_i p_i^k, \operatorname{div} \mathbf{v}) = (\tilde{\mathbf{f}}^k, \mathbf{v}),$$

$$(4b) \quad (K_i^{-1} \mathbf{w}_i^k, \mathbf{z}_i) - (p_i^k, \operatorname{div} \mathbf{z}_i) = 0, \quad i = 1, \dots, n,$$

$$(4c) \quad -(\alpha_i \operatorname{div} \mathbf{u}^k, q_i) - \tau (\operatorname{div} \mathbf{w}_i^k, q_i) - (s_i p_i^k, q_i) - \tau \left(\sum_{\substack{j=1 \\ j \neq i}}^n \xi_{ij} (p_i^k - p_j^k), q_i \right) = (\tilde{g}_i^k, q_i), \quad i = 1, \dots, n,$$

for all $(\mathbf{v}, \mathbf{z}, q) \in \mathbf{U} \times \mathbf{W} \times \mathbf{P}$, where τ denotes the time-step parameter and $\tilde{\mathbf{f}}^k := \tilde{\mathbf{f}}(\mathbf{x}, t_k)$, $\tilde{g}_i^k := -\tau \tilde{g}_i(\mathbf{x}, t_k) - \alpha_i \operatorname{div}(\mathbf{u}^{k-1}) - s_i p_i^{k-1}$ are the right hand sides.

In order to obtain a symmetric (perturbed) saddle-point problem that is handy for analysis, we apply the following similarity transformations to system (4) and substitutions: we divide (4a) by $2\tilde{\mu}$, multiply (4b) by $\frac{\alpha_i}{2\tilde{\mu}}$ and (4c) by α_i^{-1} and introduce

$$\begin{aligned} \mathbf{u} &:= \mathbf{u}^k, \quad \mathbf{w}_i := \frac{\tau}{\alpha_i} \mathbf{w}_i^k, \quad p_i := \frac{\alpha_i}{2\tilde{\mu}} p_i^k, \quad \mathbf{f} := \frac{\tilde{\mathbf{f}}^k}{2\tilde{\mu}}, \quad g_i := \alpha_i^{-1} \tilde{g}_i^k, \\ \lambda &:= \frac{\tilde{\lambda}}{2\tilde{\mu}}, \quad R_i^{-1} := \frac{\alpha_i^2}{2\tilde{\mu}\tau} K_i^{-1}, \quad \alpha_{p_i} := \frac{2\tilde{\mu}}{\alpha_i^2} s_i, \quad \xi_{ii} := \sum_{\substack{j=1 \\ j \neq i}}^n \xi_{ij}, \\ \zeta_{ii} &:= \alpha_{p_i} + \frac{2\tilde{\mu}\tau\xi_{ii}}{\alpha_i^2}, \quad \zeta_{ij} := -\frac{2\tilde{\mu}\tau\xi_{ij}}{\alpha_i\alpha_j} \text{ for } i \neq j, \quad \boldsymbol{\zeta}_i := (\zeta_{i1}, \dots, \zeta_{in})^T, \quad i = 1, \dots, n. \end{aligned}$$

Now problem (1) takes the form, cf. [13]: Find $(\mathbf{u}, \mathbf{w}, \mathbf{p}) \in \mathbf{U} \times \mathbf{W} \times \mathbf{P}$ such that

$$(5a) \quad a(\mathbf{u}, \mathbf{v}) - (\mathbf{1} \cdot \mathbf{p}, \operatorname{div} \mathbf{v}) = (\mathbf{f}, \mathbf{v}),$$

$$(5b) \quad (R_i^{-1} \mathbf{w}_i, \mathbf{z}_i) - (p_i, \operatorname{div} \mathbf{z}_i) = 0, \quad i = 1, \dots, n,$$

$$(5c) \quad -(\operatorname{div} \mathbf{u}, q_i) - (\operatorname{div} \mathbf{w}_i, q_i) - (\boldsymbol{\zeta}_i \cdot \mathbf{p}, q_i) = (g_i, q_i), \quad i = 1, \dots, n,$$

holds for all $(\mathbf{v}, \mathbf{z}, \mathbf{q}) \in \mathbf{U} \times \mathbf{W} \times \mathbf{P}$, where $\mathbf{1} = (1, \dots, 1)^T$ and

$$(6) \quad a(\mathbf{u}, \mathbf{v}) := \int_{\Omega} \boldsymbol{\epsilon}(\mathbf{u}) : \boldsymbol{\epsilon}(\mathbf{v}) \, dx + \lambda \int_{\Omega} \operatorname{div} \mathbf{u} \operatorname{div} \mathbf{v} \, dx.$$

3. HYBRIDIZED DG/HYBRID MIXED METHODS

Our goal is to generalize the hybridized DG/hybrid mixed methods, which have already been studied in [17] in the case of Biot's consolidation model. Therefore, we use a hybridized discontinuous Galerkin method for the mechanics subproblem and a hybrid mixed method for the flow subproblem.

We begin with a shape-regular triangulation \mathcal{T}_h with uniform mesh size h and the associated set of all facets \mathcal{F}_h . Then for $i = 1, \dots, n$, we define the finite element spaces

$$\begin{aligned} \mathbf{U}_h &:= \{\mathbf{v} \in \mathbf{H}_0(\operatorname{div}, \Omega) : \mathbf{v}|_T \in \mathbf{U}(T), \, T \in \mathcal{T}_h\}, \\ \mathbf{W}_{i,h} &:= \{\mathbf{z}_i \in \mathbf{H}_0(\operatorname{div}, \Omega) : \mathbf{z}_i|_T \in \mathbf{W}_i(T), \, T \in \mathcal{T}_h\}, \quad \mathbf{W}_h = \mathbf{W}_{1,h} \times \dots \times \mathbf{W}_{n,h}, \\ P_{i,h} &:= \{q_i \in L_0^2(\Omega) : q_i|_T \in P_i(T), \, T \in \mathcal{T}_h\}, \quad \mathbf{P}_h = P_{1,h} \times \dots \times P_{n,h}. \end{aligned}$$

Thereby the local spaces $\mathbf{U}(T)/\mathbf{W}_i(T)/P_i(T)$ can be chosen either as $\mathbf{BDM}_{\ell}(T)/\mathbf{RT}_{\ell-1}(T)/\mathbf{P}_{\ell-1}(T)$ or as $\mathbf{BDFM}_{\ell}(T)/\mathbf{RT}_{\ell-1}(T)/\mathbf{P}_{\ell-1}(T)$ where $\mathbf{BD}(\mathbf{F})\mathbf{M}_{\ell}(T)$, $\mathbf{RT}_{\ell-1}(T)$, and $\mathbf{P}_{\ell-1}(T)$ represent the local Brezzi-Douglas-(Fortin-)Marini space of order $\ell \geq 1$, the Raviart-Thomas space of order $\ell - 1$, and full polynomials of degree $\ell - 1$, respectively, for details, see [2].

We exploit $\mathbf{H}(\operatorname{div})$ -conforming discretizations for the mechanics subproblem since these, contrary to lower-order H^1 -conforming discretizations, allow to impose incompressibility constraints exactly on the discrete level. In particular, pointwise divergence-free solutions can be approximated and pressure robustness achieved, see [9, 8].

Next, let $\mathbf{L}^2(\mathcal{F}_h)$ be the space of the vector-valued square integrable functions on the skeleton \mathcal{F}_h and $\mathbf{P}_{\ell}(F)$ the space of vector-valued, component-wise polynomial functions of order ℓ on each facet $F \in \mathcal{F}_h$. We now introduce the spaces

$$\widehat{\mathbf{U}}_h := \{\hat{\mathbf{v}} \in \mathbf{L}^2(\mathcal{F}_h) : \hat{\mathbf{v}}|_F \in \mathbf{P}_{\ell}(F) \text{ and } \hat{\mathbf{v}}|_F \cdot \mathbf{n} = 0, \, F \in \mathcal{F}_h, \, \hat{\mathbf{v}} = \mathbf{0} \text{ on } \partial\Omega\}, \quad \overline{\mathbf{U}}_h := \mathbf{U}_h \times \widehat{\mathbf{U}}_h,$$

as well as the HDG variable $(\mathbf{u}_h, \hat{\mathbf{u}}_h) \in \overline{\mathbf{U}}_h$. The unknown $\hat{\mathbf{u}}_h$ is an approximation of the tangential trace of the displacement field \mathbf{u} and is used to weakly impose the tangential continuity, as presented in [7, 21]. Utilizing the space $\overline{\mathbf{U}}_h$, we replace the first term in the bilinear form $a(\cdot, \cdot)$ defined in (6) by $a_h^{\text{HDG}}(\cdot, \cdot)$ given by

$$(7) \quad \begin{aligned} a_h^{\text{HDG}}((\mathbf{u}, \hat{\mathbf{u}}), (\mathbf{v}, \hat{\mathbf{v}})) &:= \sum_{T \in \mathcal{T}_h} \left[\int_T \boldsymbol{\epsilon}(\mathbf{u}) : \boldsymbol{\epsilon}(\mathbf{v}) \, dx + \int_{\partial T} \boldsymbol{\epsilon}(\mathbf{u}) \mathbf{n} \cdot (\hat{\mathbf{v}} - \mathbf{v})_t \, ds \right. \\ &\quad \left. + \int_{\partial T} \boldsymbol{\epsilon}(\mathbf{v}) \mathbf{n} \cdot (\hat{\mathbf{u}} - \mathbf{u})_t \, ds + \eta \ell^2 h^{-1} \int_{\partial T} (\hat{\mathbf{u}} - \mathbf{u})_t \cdot (\hat{\mathbf{v}} - \mathbf{v})_t \, ds \right], \end{aligned}$$

where $(\mathbf{u}, \hat{\mathbf{u}}), (\mathbf{v}, \hat{\mathbf{v}}) \in \overline{\mathbf{U}}_h$ and η represents a suitable stabilization parameter independent of all model and discretization parameters. The subscript t denotes the tangential component of a vector field on a facet. Exactly divergence-free HDG methods as well as improvements to these methods are discussed in more depth in [21, 18, 19].

Using a hybrid mixed formulation for the flow subproblem allows for more efficient preconditioned iterative methods, since inverting a div-grad operator is more cost-efficient than inverting a grad-div operator. In order to construct a hybrid mixed method for the (\mathbf{w}, \mathbf{p}) system, we break up the normal continuity of the \mathbf{w} variable, i.e., placing it in the space $\mathbf{W}_h^- = \mathbf{W}_{1,h}^- \times \dots \times \mathbf{W}_{n,h}^-$ instead of the space \mathbf{W}_h , and reinforce it by a Lagrange multiplier $\hat{\mathbf{p}}_h \in \widehat{\mathbf{P}}_h = \widehat{P}_{1,h} \times \dots \times \widehat{P}_{n,h}$, where

$$\mathbf{W}_{i,h}^- := \{\mathbf{z}_i \in \mathbf{L}^2(\Omega) : \mathbf{z}_i|_T \in \mathbf{W}_i(T), \, T \in \mathcal{T}_h\}, \quad \widehat{P}_{i,h} := \prod_{F \in \mathcal{F}_h} \mathbf{P}_{\ell-1}(F), \quad \overline{P}_{i,h} := P_{i,h} \times \widehat{P}_{i,h}.$$

Here, the local space $\mathbf{W}_i(T)$ can be chosen as before. We also introduce the product space $\bar{\mathbf{P}}_h := \bar{P}_{1,h} \times \dots \times \bar{P}_{n,h}$ and define for all $\mathbf{w}_{i,h} \in \mathbf{W}_{i,h}^-$ and $(p_{i,h}, \hat{p}_{i,h}) \in \bar{P}_{i,h}$ the bilinear form

$$(8) \quad b(\mathbf{w}_{i,h}, (p_{i,h}, \hat{p}_{i,h})) = \sum_{T \in \mathcal{T}_h} \left(\int_T \operatorname{div} \mathbf{w}_{i,h} p_{i,h} \, dx - \int_{\partial T} \mathbf{w}_{i,h} \cdot \mathbf{n} \hat{p}_{i,h} \, ds \right), \quad i = 1, \dots, n.$$

Note that the space \mathbf{W}_h^- is a discontinuous version of \mathbf{W}_h and that $\hat{\mathbf{P}}_h$ has been chosen as the normal trace space of \mathbf{W}_h .

With these spaces and bilinear forms at hand, we formulate the following HDG hybrid mixed finite element method for (5): Find $((\mathbf{u}_h, \hat{\mathbf{u}}_h), \mathbf{w}_h, (\mathbf{p}_h, \hat{\mathbf{p}}_h)) \in \bar{\mathbf{U}}_h \times \mathbf{W}_h^- \times \bar{\mathbf{P}}_h$ such that

$$(9a) \quad a_h((\mathbf{u}_h, \hat{\mathbf{u}}_h), (\mathbf{v}_h, \hat{\mathbf{v}}_h)) - (\mathbf{1} \cdot \mathbf{p}_h, \operatorname{div} \mathbf{v}_h) = (\mathbf{f}, \mathbf{v}_h),$$

$$(9b) \quad (R_i^{-1} \mathbf{w}_{i,h}, \mathbf{z}_{i,h}) - b(\mathbf{z}_{i,h}, (p_{i,h}, \hat{p}_{i,h})) = 0, \quad i = 1, \dots, n,$$

$$(9c) \quad -(\operatorname{div} \mathbf{u}_h, q_{i,h}) - b(\mathbf{w}_{i,h}, (q_{i,h}, \hat{q}_{i,h})) - (\boldsymbol{\zeta}_i \cdot \mathbf{p}_h, q_{i,h}) = (g_i, q_{i,h}), \quad i = 1, \dots, n,$$

holds for all $((\mathbf{v}_h, \hat{\mathbf{v}}_h), \mathbf{z}_h, (\mathbf{q}_h, \hat{\mathbf{q}}_h)) \in \bar{\mathbf{U}}_h \times \mathbf{W}_h^- \times \bar{\mathbf{P}}_h$, where

$$(10) \quad a_h((\mathbf{u}_h, \hat{\mathbf{u}}_h), (\mathbf{v}_h, \hat{\mathbf{v}}_h)) := a_h^{\text{HDG}}((\mathbf{u}_h, \hat{\mathbf{u}}_h), (\mathbf{v}_h, \hat{\mathbf{v}}_h)) + \lambda \int_{\Omega} \operatorname{div} \mathbf{u}_h \operatorname{div} \mathbf{v}_h \, dx.$$

Next, we want to prove the parameter-robust stability for the methods just introduced.

4. STABILITY ANALYSIS

This section is devoted to the well-posedness analysis of the discrete problem (9) resulting from application of the HDG hybrid mixed method. To begin with, we introduce in Section 4.1 parameter-dependant norms, first on the continuous and then on the discrete level on which we will also define the related combined norm $\|\cdot\|_{\bar{\mathbf{X}}_h}$. The latter provides a norm-equivalent preconditioner for (9). To prove parameter-robust well-posedness, in Section 4.2, and, in particular, inf-sup stability, we use a specific norm fitting technique that has recently been introduced in [14]. This will give rise to a different discrete norm $\|\cdot\|_{\mathbf{Y}_h}$ which will be proven to be equivalent to $\|\cdot\|_{\bar{\mathbf{X}}_h}$ at the end of this section.

4.1. Parameter-dependent norms. In this subsection, we introduce the parameter-dependent norms for the construction of norm-equivalent operator preconditioners.

To this end, let us define the following parameter matrices

$$(11) \quad \Lambda_{\zeta} := \{\zeta_{ij}\}_{i,j=1}^n, \quad \Lambda := \Lambda_{\zeta} + \frac{1}{\lambda_0} \mathbb{I},$$

where $\lambda_0 := \max\{1, \lambda\}$ and \mathbb{I} is the matrix of all ones. By $\|\cdot\|_0$ we denote the L^2 -norm for scalar as well as vector-valued functions.

Note that $\Lambda + RI$ is a symmetric positive definite matrix and so is $(\Lambda + RI)^{-1}$, where $R := \min\{R_1, \dots, R_n\}$ and I denotes the identity matrix. The Hilbert spaces $\mathbf{U}, \mathbf{W}, \mathbf{P}$ are equipped with the inner products

$$(12a) \quad (\mathbf{u}, \mathbf{v})_{\mathbf{U}} := (\boldsymbol{\epsilon}(\mathbf{u}), \boldsymbol{\epsilon}(\mathbf{v})) + \lambda(\operatorname{div} \mathbf{u}, \operatorname{div} \mathbf{v}),$$

$$(12b) \quad (\mathbf{w}, \mathbf{z})_{\mathbf{W}} := \sum_{i=1}^n (R_i^{-1} \mathbf{w}_i, \mathbf{z}_i) + ((\Lambda + RI)^{-1} \operatorname{Div} \mathbf{w}, \operatorname{Div} \mathbf{z}),$$

$$(12c) \quad (\mathbf{w}, \mathbf{z})_{\mathbf{W}^-} := \sum_{i=1}^n (R_i^{-1} \mathbf{w}_i, \mathbf{z}_i),$$

$$(12d) \quad (\mathbf{p}, \mathbf{q})_{\mathbf{P}} := \sum_{i=1}^n R_i(p_i, q_i) + (\Lambda \mathbf{p}, \mathbf{q}),$$

where $(\text{Div } \mathbf{w})^T = (\text{div } \mathbf{w}_1, \dots, \text{div } \mathbf{w}_n)$ and the induced norms $\|\cdot\|_{\mathbf{U}}$, $\|\cdot\|_{\mathbf{W}}$, $\|\cdot\|_{\mathbf{W}^-}$ and $\|\cdot\|_{\mathbf{P}}$, respectively.

Next, we introduce several discrete norms. The hybridized discontinuous Galerkin (HDG) norm on the displacement product space $\overline{\mathbf{U}}_h$ is defined by

$$(13) \quad \|(\mathbf{v}_h, \hat{\mathbf{v}}_h)\|_{\mathbf{HDG}}^2 := \sum_{T \in \mathcal{T}_h} (\|\boldsymbol{\epsilon}(\mathbf{v}_h)\|_{0,T}^2 + h^{-1} \|(\hat{\mathbf{v}}_h - \mathbf{v}_h)_t\|_{0,\partial T}^2 + h^2 |\mathbf{v}_h|_{2,T}^2),$$

and can be used to obtain the following discrete norm

$$(14) \quad \|(\mathbf{v}_h, \hat{\mathbf{v}}_h)\|_{\overline{\mathbf{U}}_h}^2 := \|(\mathbf{v}_h, \hat{\mathbf{v}}_h)\|_{\mathbf{HDG}}^2 + \lambda \|\text{div } \mathbf{v}_h\|_0^2.$$

Further, we introduce the HDG norm $\|\cdot\|_{\mathbf{HDG}}$ on the pressure product space $\overline{\mathbf{P}}_h$ by

$$(15) \quad \|(q_h, \hat{q}_h)\|_{\mathbf{HDG}}^2 := \sum_{T \in \mathcal{T}_h} (\|\nabla q_h\|_{0,T}^2 + h^{-1} \|\hat{q}_h - q_h\|_{0,\partial T}^2 + h^2 |q_h|_{2,T}^2),$$

and the related norm $\|\cdot\|_{\overline{\mathbf{P}}_h}$ by

$$(16) \quad \|(\mathbf{q}_h, \hat{\mathbf{q}}_h)\|_{\overline{\mathbf{P}}_h}^2 := \sum_{i=1}^n R_i \|(q_{i,h}, \hat{q}_{i,h})\|_{\mathbf{HDG}}^2 + (\Lambda \mathbf{q}_h, \mathbf{q}_h).$$

Finally, we denote the product space

$$(17) \quad \overline{\mathbf{X}}_h := \overline{\mathbf{U}}_h \times \mathbf{W}_h^- \times \overline{\mathbf{P}}_h,$$

and equip it with the norm

$$(18) \quad \|((\mathbf{v}_h, \hat{\mathbf{v}}_h), \mathbf{z}_h, (\mathbf{q}_h, \hat{\mathbf{q}}_h))\|_{\overline{\mathbf{X}}_h}^2 := \|(\mathbf{v}_h, \hat{\mathbf{v}}_h)\|_{\overline{\mathbf{U}}_h}^2 + \|\mathbf{z}_h\|_{\mathbf{W}^-}^2 + \|(\mathbf{q}_h, \hat{\mathbf{q}}_h)\|_{\overline{\mathbf{P}}_h}^2.$$

4.2. Parameter-robust well-posedness. In this subsection, we generalize our result from [17] herewith showing the uniform well-posedness of (9).

Before we explain what uniformly well-posedness means and why it is important, we recall an abstract stability result based on a specific norm fitting, as it has recently been presented in [14]. To this end, we present (9) as a perturbed saddle-point problem of the form

$$(19) \quad \mathbf{A}_h((\mathbf{u}_h, \mathbf{p}_h), (\mathbf{v}_h, \mathbf{q}_h)) = \mathbf{F}_h((\mathbf{v}_h, \mathbf{q}_h)) \quad \forall \mathbf{v}_h \in \mathbf{V}_h, \forall \mathbf{q}_h \in \mathbf{Q}_h,$$

where $\mathbf{V}_h := \overline{\mathbf{U}}_h \times \mathbf{W}_h^-$, $\mathbf{Q}_h := \overline{\mathbf{P}}_h$, $\mathbf{u}_h := ((\mathbf{u}_h, \hat{\mathbf{u}}_h), \mathbf{w}_h)$, $\mathbf{v}_h := ((\mathbf{v}_h, \hat{\mathbf{v}}_h), \mathbf{z}_h)$, $\mathbf{p}_h := (\mathbf{p}_h, \hat{\mathbf{p}}_h)$, $\mathbf{q}_h := (\mathbf{q}_h, \hat{\mathbf{q}}_h)$ and the bilinear form $\mathbf{A}_h((\cdot, \cdot), (\cdot, \cdot))$ has the representation

$$(20) \quad \mathbf{A}_h((\mathbf{u}_h, \mathbf{p}_h), (\mathbf{v}_h, \mathbf{q}_h)) = \mathbf{a}_h(\mathbf{u}_h, \mathbf{v}_h) + \mathbf{b}_h(\mathbf{v}_h, \mathbf{p}_h) + \mathbf{b}_h(\mathbf{u}_h, \mathbf{q}_h) - \mathbf{c}(\mathbf{p}_h, \mathbf{q}_h),$$

in terms of the bilinear forms $\mathbf{a}_h(\cdot, \cdot)$, $\mathbf{b}_h(\cdot, \cdot)$ and $\mathbf{c}(\cdot, \cdot)$. Each of these bilinear forms can be associated with a bounded linear operator as given by

$$(21a) \quad \mathbf{A} : \mathbf{V}_h \rightarrow \mathbf{V}_h' : \langle \mathbf{A} \mathbf{u}_h, \mathbf{v}_h \rangle_{\mathbf{V}_h' \times \mathbf{V}_h} = \mathbf{a}_h(\mathbf{u}_h, \mathbf{v}_h), \quad \forall \mathbf{u}_h, \mathbf{v}_h \in \mathbf{V}_h,$$

$$(21b) \quad \mathbf{C} : \mathbf{Q}_h \rightarrow \mathbf{Q}_h' : \langle \mathbf{C} \mathbf{p}_h, \mathbf{q}_h \rangle_{\mathbf{Q}_h' \times \mathbf{Q}_h} = \mathbf{c}(\mathbf{p}_h, \mathbf{q}_h), \quad \forall \mathbf{p}_h, \mathbf{q}_h \in \mathbf{Q}_h,$$

$$(21c) \quad \mathbf{B} : \mathbf{V}_h \rightarrow \mathbf{Q}_h' : \langle \mathbf{B} \mathbf{v}_h, \mathbf{q}_h \rangle_{\mathbf{Q}_h' \times \mathbf{Q}_h} = \mathbf{b}_h(\mathbf{v}_h, \mathbf{q}_h), \quad \forall \mathbf{v}_h \in \mathbf{V}_h, \forall \mathbf{q}_h \in \mathbf{Q}_h,$$

$$(21d) \quad \mathbf{B}^T : \mathbf{Q}_h \rightarrow \mathbf{V}_h' : \langle \mathbf{B}^T \mathbf{q}_h, \mathbf{v}_h \rangle_{\mathbf{V}_h' \times \mathbf{V}_h} = \mathbf{b}_h(\mathbf{v}_h, \mathbf{q}_h), \quad \forall \mathbf{v}_h \in \mathbf{V}_h, \forall \mathbf{q}_h \in \mathbf{Q}_h,$$

where \mathbf{V}_h' and \mathbf{Q}_h' denote the dual spaces of \mathbf{V}_h and \mathbf{Q}_h , respectively, and $\langle \cdot, \cdot \rangle_{\mathbf{V}_h' \times \mathbf{V}_h}$ as well as $\langle \cdot, \cdot \rangle_{\mathbf{Q}_h' \times \mathbf{Q}_h}$ the corresponding duality pairings.

Next we introduce the abstract norm $\|\cdot\|_{\mathbf{Q}_h}$ on the space \mathbf{Q}_h and the abstract norm $\|\cdot\|_{\mathbf{V}_h}$ on \mathbf{V}_h which have the following representations, see [14],

$$(22) \quad \|\mathbf{q}_h\|_{\mathbf{Q}_h}^2 := |\mathbf{q}_h|_{\mathbf{Q}_h}^2 + \mathbf{c}(\mathbf{q}_h, \mathbf{q}_h) =: \langle \bar{\mathbf{Q}} \mathbf{q}_h, \mathbf{q}_h \rangle_{\mathbf{Q}_h' \times \mathbf{Q}_h},$$

and

$$(23) \quad \|\mathbf{v}_h\|_{\mathbf{V}_h}^2 := |\mathbf{v}_h|_{\mathbf{V}_h}^2 + |\mathbf{v}_h|_{\mathbf{b}}^2.$$

Assuming that the seminorm $|\cdot|_{\mathbf{Q}_h}^2$ is defined via a symmetric positive semidefinite (SPSD) bilinear form $d(\cdot, \cdot)$, i.e., $|\mathbf{q}_h|_{\mathbf{Q}_h}^2 = d(\mathbf{q}_h, \mathbf{q}_h)$ and $(c(\cdot, \cdot) + d(\cdot, \cdot))$ is symmetric positive definite (SPD), the operator $\bar{Q} : \mathbf{Q}_h \rightarrow \mathbf{Q}'_h$ is a linear invertible operator, the Riesz isomorphism corresponding to the inner product $(\cdot, \cdot)_{\mathbf{Q}_h}$ inducing the norm $\|\cdot\|_{\mathbf{Q}_h}$. Moreover, $|\cdot|_{\mathbf{V}_h}$ is a proper seminorm, which is a norm on $\text{Ker}(B)$ satisfying

$$|\mathbf{v}_h|_{\mathbf{V}_h}^2 \approx \mathbf{a}_h(\mathbf{v}_h, \mathbf{v}_h) \quad \forall \mathbf{v}_h \in \text{Ker}(B),$$

and $|\cdot|_{\mathbf{b}}$ is defined by

$$(24) \quad |\mathbf{v}_h|_{\mathbf{b}}^2 := \langle B\mathbf{v}_h, \bar{Q}^{-1}B\mathbf{v}_h \rangle_{\mathbf{Q}'_h \times \mathbf{Q}_h}.$$

Note that $\bar{Q}^{-1} : \mathbf{Q}'_h \rightarrow \mathbf{Q}_h$ is an isometric isomorphism and it is fulfilled that

$$\begin{aligned} \langle B\mathbf{v}_h, \bar{Q}^{-1}B\mathbf{v}_h \rangle_{\mathbf{Q}'_h \times \mathbf{Q}_h} &= \langle \bar{Q}\bar{Q}^{-1}B\mathbf{v}_h, \bar{Q}^{-1}B\mathbf{v}_h \rangle_{\mathbf{Q}'_h \times \mathbf{Q}_h} \\ &= (\bar{Q}^{-1}B\mathbf{v}_h, \bar{Q}^{-1}B\mathbf{v}_h)_{\mathbf{Q}_h} = \|\bar{Q}^{-1}B\mathbf{v}_h\|_{\mathbf{Q}_h}^2 = \|B\mathbf{v}_h\|_{\mathbf{Q}'_h}^2. \end{aligned}$$

Additionally, we introduce the product space $\mathbf{Y}_h := \mathbf{V}_h \times \mathbf{Q}_h$ and equip it with the norm $\|\cdot\|_{\mathbf{Y}_h}$ defined by

$$(25) \quad \|\mathbf{y}_h\|_{\mathbf{Y}_h}^2 = \|\mathbf{v}_h\|_{\mathbf{V}_h}^2 + \|\mathbf{q}_h\|_{\mathbf{Q}_h}^2, \quad \forall \mathbf{y}_h = (\mathbf{v}_h, \mathbf{q}_h) \in \mathbf{Y}_h.$$

Then the following theorem is an analogue to Brezzi's splitting theorem for the abstract perturbed saddle-point problem (19)–(20).

Theorem 1. *Let $\|\cdot\|_{\mathbf{V}_h}$ and $\|\cdot\|_{\mathbf{Q}_h}$ be defined according to (22)–(23) and consider the bilinear form $A_h((\cdot, \cdot), (\cdot, \cdot))$ from (20) for which $\mathbf{a}_h(\cdot, \cdot)$ is continuous and $\mathbf{a}_h(\cdot, \cdot)$ and $\mathbf{c}(\cdot, \cdot)$ are symmetric positive semidefinite.*

Further, assume that $\mathbf{a}_h(\cdot, \cdot)$ satisfies the coercivity estimate

$$(26) \quad \mathbf{a}_h(\mathbf{v}_h, \mathbf{v}_h) \geq \underline{C}_a |\mathbf{v}_h|_{\mathbf{V}_h}^2, \quad \forall \mathbf{v}_h \in \mathbf{V}_h,$$

and that there exists a constant $\underline{\beta} > 0$ such that

$$(27) \quad \sup_{\substack{\mathbf{v}_h \in \mathbf{V}_h \\ \mathbf{v}_h \neq 0}} \frac{\mathbf{b}_h(\mathbf{v}_h, \mathbf{q}_h)}{\|\mathbf{v}_h\|_{\mathbf{V}_h}} \geq \underline{\beta} |\mathbf{q}_h|_{\mathbf{Q}_h}, \quad \forall \mathbf{q}_h \in \mathbf{Q}_h.$$

Then the bilinear form $A_h((\cdot, \cdot), (\cdot, \cdot))$ is continuous and inf-sup stable under the combined norm $\|\cdot\|_{\mathbf{Y}_h}$ defined in (25), i.e., the conditions

$$(28) \quad A_h(\mathbf{x}_h, \mathbf{y}_h) \leq \bar{C} \|\mathbf{x}_h\|_{\mathbf{Y}_h} \|\mathbf{y}_h\|_{\mathbf{Y}_h}, \quad \forall \mathbf{x}_h, \mathbf{y}_h \in \mathbf{Y}_h,$$

and

$$(29) \quad \inf_{\mathbf{x}_h \in \mathbf{Y}_h} \sup_{\mathbf{y}_h \in \mathbf{Y}_h} \frac{A_h(\mathbf{x}_h, \mathbf{y}_h)}{\|\mathbf{x}_h\|_{\mathbf{Y}_h} \|\mathbf{y}_h\|_{\mathbf{Y}_h}} \geq \underline{\alpha} > 0$$

hold, where $\mathbf{x}_h := (\mathbf{u}_h, \mathbf{p}_h)$.

Proof. The proof of this result is given in [14]. □

Furthermore, the following Lemmas, the proofs of which can be found in [17], are essential for showing the well-posedness of (9).

Lemma 2. *There holds the following discrete inf-sup condition*

$$(30) \quad \inf_{(q_1, \dots, q_n, h) \in \mathcal{P}_h} \sup_{(\mathbf{v}_h, \hat{\mathbf{v}}_h) \in \bar{\mathcal{U}}_h} \frac{(\operatorname{div} \mathbf{v}_h, \sum_{i=1}^n q_{i,h})}{\|(\mathbf{v}_h, \hat{\mathbf{v}}_h)\|_{\mathbf{HDG}} \|\sum_{i=1}^n q_{i,h}\|_0} \geq \beta_{S,d} > 0,$$

where $\beta_{S,d}$ is a constant independent of all problem parameters.

Lemma 3. *There hold the following discrete inf-sup conditions*

$$(31) \quad \inf_{(q_{i,h}, \hat{q}_{i,h}) \in \bar{\mathcal{P}}_{i,h}} \sup_{\mathbf{z}_{i,h} \in \mathbf{W}_{i,h}^-} \frac{b(\mathbf{z}_{i,h}, (q_{i,h}, \hat{q}_{i,h}))}{\|\mathbf{z}_{i,h}\|_0 \|(q_{i,h}, \hat{q}_{i,h})\|_{\mathbf{HDG}}} \geq \beta_{D,d} > 0, \quad i = 1, \dots, n,$$

where $\beta_{D,d}$ is a constant independent of all problem parameters.

For our problem at hand, we identify the small bilinear forms introduced in (20) by

$$(32a) \quad \mathbf{a}_h(\mathbf{u}_h, \mathbf{v}_h) := a_h((\mathbf{u}_h, \hat{\mathbf{u}}_h), (\mathbf{v}_h, \hat{\mathbf{v}}_h)) + \sum_{i=1}^n (R_i^{-1} \mathbf{w}_{i,h}, \mathbf{z}_{i,h}),$$

$$(32b) \quad \mathbf{b}_h(\mathbf{v}_h, \mathbf{p}_h) := -(\mathbf{1} \cdot \mathbf{p}_h, \operatorname{div} \mathbf{v}_h) - \sum_{i=1}^n b(\mathbf{z}_{i,h}, (p_{i,h}, \hat{p}_{i,h})),$$

$$(32c) \quad \mathbf{c}(\mathbf{p}_h, \mathbf{q}_h) := \sum_{i=1}^n (\zeta_i \cdot \mathbf{p}_h, q_{i,h}) = (\Lambda_\zeta \mathbf{p}_h, \mathbf{q}_h),$$

and the linear form by

$$(33) \quad \mathbf{F}_h((\mathbf{v}_h, \mathbf{q}_h)) = (\mathbf{f}, \mathbf{v}_h) + \sum_{i=1}^n (g_i, q_{i,h}).$$

Next we specify the fitted norms in which problem (9) will be analyzed. To this end, consider

$$(34) \quad |\mathbf{q}_h|_{\mathcal{Q}_h}^2 := \sum_{i=1}^n R_i \|(q_{i,h}, \hat{q}_{i,h})\|_{\mathbf{HDG}}^2 + \frac{1}{\lambda_0} \left\| \sum_{i=1}^n q_{i,h} \right\|_0^2, \quad \forall \mathbf{q}_h = (q_h, \hat{q}_h) \in \mathcal{Q}_h,$$

$$(35) \quad |\mathbf{v}_h|_{\mathbf{V}_h}^2 := a_h^{\mathbf{HDG}}((\mathbf{v}_h, \hat{\mathbf{v}}_h), (\mathbf{v}_h, \hat{\mathbf{v}}_h)) + \lambda \|\operatorname{div} \mathbf{v}_h\|_0^2 + \sum_{i=1}^n R_i^{-1} \|\mathbf{z}_{i,h}\|_0^2 \\ = \mathbf{a}_h(\mathbf{v}_h, \mathbf{v}_h), \quad \forall \mathbf{v}_h = ((\mathbf{v}_h, \hat{\mathbf{v}}_h), \mathbf{z}_h) \in \mathbf{V}_h,$$

which are to be used together with (32) in the definitions (22) and (23).

Definition 1. *We call the problem (19) uniformly well-posed under the norm $\|\cdot\|_{\mathbf{Y}_h}$ defined by (25) if the conditions of Theorem 1 are satisfied and the constants \bar{C} and $\underline{\alpha}$ in (28) and (29) are independent of all problem parameters.*

Theorem 4. *Problem (9) is uniformly well-posed under the norm (25) where $\|\cdot\|_{\mathcal{Q}_h}$ and $\|\cdot\|_{\mathbf{V}_h}$ are based on (34) and (35), respectively.*

Proof. Obviously, the coercivity estimate (26) is fulfilled with $\underline{C}_a = 1$. We next show that (27) holds. From the inf-sup conditions (30) and (31), we get that for $(q_h, \hat{q}_h) \in \mathcal{Q}_h$ there exists $\mathbf{v}_{h,0} = ((\mathbf{v}_{h,0}, \hat{\mathbf{v}}_{h,0}), \mathbf{z}_{h,0}) \in \mathbf{V}_h$ such that

$$(36) \quad -\operatorname{div} \mathbf{v}_{h,0} = \frac{1}{\lambda_0} \sum_{i=1}^n q_{i,h} \quad \text{and} \quad \|(\mathbf{v}_{h,0}, \hat{\mathbf{v}}_{h,0})\|_{\mathbf{HDG}}^2 \leq \beta_{S,d}^{-2} \frac{1}{\lambda_0^2} \left\| \sum_{i=1}^n q_{i,h} \right\|_0^2,$$

and

$$(37) \quad -b(\mathbf{z}_{i,h,0}, (q_{i,h}, \hat{q}_{i,h})) = R_i \|(q_{i,h}, \hat{q}_{i,h})\|_{\mathbf{HDG}}^2 \quad \text{and} \quad \|\mathbf{z}_{i,h,0}\|_0^2 \leq \beta_{D,d}^{-2} R_i^2 \|(q_{i,h}, \hat{q}_{i,h})\|_{\mathbf{HDG}}^2.$$

Now we can infer

$$\begin{aligned}
(38) \quad \beta_{S,d}^{-2} \frac{1}{\lambda_0} \left\| \sum_{i=1}^n q_{i,h} \right\|_0^2 &\geq \frac{1}{2} \lambda_0 \left[\|(\mathbf{v}_{h,0}, \hat{\mathbf{v}}_{h,0})\|_{\text{HDG}}^2 + \|(\mathbf{v}_{h,0}, \hat{\mathbf{v}}_{h,0})\|_{\text{HDG}}^2 \right] \\
&\geq \frac{1}{2\bar{C}_a} \lambda_0 a_h^{\text{HDG}}((\mathbf{v}_{h,0}, \hat{\mathbf{v}}_{h,0}), (\mathbf{v}_{h,0}, \hat{\mathbf{v}}_{h,0})) + \frac{1}{2} \lambda_0 \|\operatorname{div} \mathbf{v}_{h,0}\|_0^2 \\
&\geq \frac{1}{2C} \left[a_h^{\text{HDG}}((\mathbf{v}_{h,0}, \hat{\mathbf{v}}_{h,0}), (\mathbf{v}_{h,0}, \hat{\mathbf{v}}_{h,0})) + 2\lambda_0 \|\operatorname{div} \mathbf{v}_{h,0}\|_0^2 \right],
\end{aligned}$$

where $C = \max\{2, \bar{C}_a\}$ and \bar{C}_a is the boundedness constant for $a_h^{\text{HDG}}((\cdot, \cdot), (\cdot, \cdot))$. Furthermore, we get

$$\beta_{D,d}^{-2} R_i \|(q_{i,h}, \hat{q}_{i,h})\|_{\text{HDG}}^2 \geq R_i^{-1} \|\mathbf{z}_{i,h,0}\|_0^2,$$

which implies

$$(39) \quad \beta_{D,d}^{-2} \sum_{i=1}^n R_i \|(q_{i,h}, \hat{q}_{i,h})\|_{\text{HDG}}^2 \geq \sum_{i=1}^n R_i^{-1} \|\mathbf{z}_{i,h,0}\|_0^2.$$

Using the Cauchy-Schwarz inequality, we obtain

$$\begin{aligned}
\sum_{i=1}^n b(\mathbf{z}_{i,h}, (q_{i,h}, \hat{q}_{i,h})) &\leq \sum_{i=1}^n C_b R_i^{1/2} \|(q_{i,h}, \hat{q}_{i,h})\|_{\text{HDG}} R_i^{-1/2} \|\mathbf{z}_{i,h}\|_0 \\
&\leq C_b \left(\sum_{i=1}^n R_i \|(q_{i,h}, \hat{q}_{i,h})\|_{\text{HDG}}^2 \right)^{1/2} \left(\sum_{i=1}^n R_i^{-1} \|\mathbf{z}_{i,h}\|_0^2 \right)^{1/2} \\
&\leq C_b \|\mathbf{q}_h\|_{\mathbf{Q}_h} \left(\sum_{i=1}^n R_i^{-1} \|\mathbf{z}_{i,h}\|_0^2 \right)^{1/2},
\end{aligned}$$

where C_b is the boundedness constant of $b(\cdot, (\cdot, \cdot))$. With this inequality, we conclude

$$\begin{aligned}
|\mathbf{v}_h|_{\mathbf{b}}^2 &= \|B\mathbf{v}_h\|_{\mathbf{Q}'_h}^2 = \left(\sup_{\substack{\mathbf{q}_h \in \mathbf{Q}_h \\ \mathbf{q}_h \neq 0}} \frac{\mathbf{b}_h(\mathbf{v}_h, \mathbf{q}_h)}{\|\mathbf{q}_h\|_{\mathbf{Q}_h}} \right)^2 \\
&= \left(\sup_{\substack{\mathbf{q}_h \in \mathbf{Q}_h \\ \mathbf{q}_h \neq 0}} \frac{-(\sum_{i=1}^n q_{i,h}, \operatorname{div} \mathbf{v}_h) - \sum_{i=1}^n b(\mathbf{z}_{i,h}, (q_{i,h}, \hat{q}_{i,h}))}{\|\mathbf{q}_h\|_{\mathbf{Q}_h}} \right)^2 \\
(40) \quad &\leq \left(\sup_{\substack{\mathbf{q}_h \in \mathbf{Q}_h \\ \mathbf{q}_h \neq 0}} \frac{\|\sum_{i=1}^n q_{i,h}\|_0 \|\operatorname{div} \mathbf{v}_h\|_0 + C_b \|\mathbf{q}_h\|_{\mathbf{Q}_h} (\sum_{i=1}^n R_i^{-1} \|\mathbf{z}_{i,h}\|_0^2)^{1/2}}{\|\mathbf{q}_h\|_{\mathbf{Q}_h}} \right)^2 \\
&\leq \left(\sup_{\substack{\mathbf{q}_h \in \mathbf{Q}_h \\ \mathbf{q}_h \neq 0}} \frac{\bar{C}_b \sqrt{\lambda_0} \|\mathbf{q}_h\|_{\mathbf{Q}_h} \|\operatorname{div} \mathbf{v}_h\|_0 + \bar{C}_b \|\mathbf{q}_h\|_{\mathbf{Q}_h} (\sum_{i=1}^n R_i^{-1} \|\mathbf{z}_{i,h}\|_0^2)^{1/2}}{\|\mathbf{q}_h\|_{\mathbf{Q}_h}} \right)^2 \\
&\leq 2\bar{C}_b^2 \left(\lambda_0 \|\operatorname{div} \mathbf{v}_h\|_0^2 + \sum_{i=1}^n R_i^{-1} \|\mathbf{z}_{i,h}\|_0^2 \right),
\end{aligned}$$

where $\bar{C}_b = \max\{1, C_b\}$.

Utilizing (38) – (40) together with the choice $\beta_d := \min \left\{ \beta_{D,d}, \frac{\beta_{S,d}}{\sqrt{2C}} \right\}$, we receive the estimate

$$\begin{aligned}
\beta_d^{-2} |\mathbf{q}_h|_{\mathbf{Q}_h}^2 &= \beta_d^{-2} \left(\sum_{i=1}^n R_i \| (q_{i,h}, \hat{q}_{i,h}) \|_{\text{HDG}}^2 + \frac{1}{\lambda_0} \left\| \sum_{i=1}^n q_{i,h} \right\|_0^2 \right) \\
&\geq \sum_{i=1}^n R_i^{-1} \| \mathbf{z}_{i,h,0} \|_0^2 + a_h^{\text{HDG}}((\mathbf{v}_{h,0}, \hat{\mathbf{v}}_{h,0}), (\mathbf{v}_{h,0}, \hat{\mathbf{v}}_{h,0})) + 2\lambda_0 \| \operatorname{div} \mathbf{v}_{h,0} \|_0^2 \\
&\geq \frac{1}{2} \sum_{i=1}^n R_i^{-1} \| \mathbf{z}_{i,h,0} \|_0^2 + a_h((\mathbf{v}_{h,0}, \hat{\mathbf{v}}_{h,0}), (\mathbf{v}_{h,0}, \hat{\mathbf{v}}_{h,0})) + \lambda_0 \| \operatorname{div} \mathbf{v}_{h,0} \|_0^2 \\
&\quad + \frac{1}{2} \sum_{i=1}^n R_i^{-1} \| \mathbf{z}_{i,h,0} \|_0^2 \\
&\geq \frac{1}{2} \left(\mathbf{a}_h(\mathbf{v}_{h,0}, \mathbf{v}_{h,0}) + \lambda_0 \| \operatorname{div} \mathbf{v}_{h,0} \|_0^2 + \sum_{i=1}^n R_i^{-1} \| \mathbf{z}_{i,h,0} \|_0^2 \right) \\
(41) \quad &\geq \frac{1}{4\bar{C}_b^2} (|\mathbf{v}_{h,0}|_{\mathbf{V}_h}^2 + |\mathbf{v}_{h,0}|_{\mathbf{b}}^2) = \frac{1}{4\bar{C}_b^2} \| \mathbf{v}_{h,0} \|_{\mathbf{V}_h}^2.
\end{aligned}$$

Finally, using (36) and (37) we deduce

$$\sup_{\substack{\mathbf{v}_h \in \mathbf{V}_h \\ \mathbf{v}_h \neq 0}} \frac{\mathbf{b}_h(\mathbf{v}_h, \mathbf{q}_h)}{\| \mathbf{v}_h \|_{\mathbf{V}_h}} \geq \frac{\mathbf{b}_h(\mathbf{v}_{h,0}, \mathbf{q}_h)}{\| \mathbf{v}_{h,0} \|_{\mathbf{V}_h}} = \frac{|\mathbf{q}_h|_{\mathbf{Q}_h}^2}{\| \mathbf{v}_{h,0} \|_{\mathbf{V}_h}} \geq \frac{1}{2} \bar{C}_b^{-1} \beta_d \frac{|\mathbf{q}_h|_{\mathbf{Q}_h}^2}{|\mathbf{q}_h|_{\mathbf{Q}_h}}.$$

□

We now show uniform well-posedness of problem (9) in the $\| \cdot \|_{\bar{\mathbf{X}}_h}$ norm. To this end, we prove that the norms $\| \cdot \|_{\mathbf{Y}_h}$ and $\| \cdot \|_{\bar{\mathbf{X}}_h}$ are equivalent with constants independent of all model and discretization parameters. The latter norm is then used in Section 5 to set up parameter-robust preconditioners.

Corollary 5. *Problem (9) is uniformly well-posed under the norm (18).*

Proof. We proof this by showing norm equivalence of the norms $\| \cdot \|_{\mathbf{Y}_h}$ and $\| \cdot \|_{\bar{\mathbf{X}}_h}$ with parameter-independent constants. For the first estimate, we exploit (40) in order to get

$$\begin{aligned}
\| (\mathbf{v}_h, \mathbf{q}_h) \|_{\mathbf{Y}_h}^2 &= |\mathbf{q}_h|_{\mathbf{Q}_h}^2 + \mathbf{c}(\mathbf{q}_h, \mathbf{q}_h) + |\mathbf{v}_h|_{\mathbf{V}_h}^2 + |\mathbf{v}_h|_{\mathbf{b}}^2 \\
&\leq \sum_{i=1}^n R_i \| (q_{i,h}, \hat{q}_{i,h}) \|_{\text{HDG}}^2 + \frac{1}{\lambda_0} \left\| \sum_{i=1}^n q_{i,h} \right\|_0^2 + (\Lambda_\zeta \mathbf{q}_h, \mathbf{q}_h) \\
&\quad + a_h^{\text{HDG}}((\mathbf{v}_h, \hat{\mathbf{v}}_h), (\mathbf{v}_h, \hat{\mathbf{v}}_h)) + \lambda \| \operatorname{div} \mathbf{v}_h \|_0^2 + \sum_{i=1}^n R_i^{-1} \| \mathbf{z}_{i,h} \|_0^2 \\
&\quad + 2\bar{C}_b^2 \left(\lambda_0 \| \operatorname{div} \mathbf{v}_h \|_0^2 + \sum_{i=1}^n R_i^{-1} \| \mathbf{z}_{i,h} \|_0^2 \right) \\
&\leq \| (\mathbf{q}_h, \hat{\mathbf{q}}_h) \|_{\bar{\mathbf{P}}_h}^2 + \bar{C}_a \| (\mathbf{v}_h, \hat{\mathbf{v}}_h) \|_{\text{HDG}}^2 + \lambda \| \operatorname{div} \mathbf{v}_h \|_0^2 + \| \mathbf{z}_h \|_{\mathbf{W}^-}^2 \\
&\quad + 2\bar{C}_b^2 (\| (\mathbf{v}_h, \hat{\mathbf{v}}_h) \|_{\text{HDG}}^2 + \lambda \| \operatorname{div} \mathbf{v}_h \|_0^2 + \| \mathbf{z}_h \|_{\mathbf{W}^-}^2) \\
&\leq C (\| (\mathbf{q}_h, \hat{\mathbf{q}}_h) \|_{\bar{\mathbf{P}}_h}^2 + \| (\mathbf{v}_h, \hat{\mathbf{v}}_h) \|_{\bar{\mathbf{U}}_h}^2 + \| \mathbf{z}_h \|_{\mathbf{W}^-}^2) \\
&= C \| ((\mathbf{v}_h, \hat{\mathbf{v}}_h), \mathbf{z}_h, (\mathbf{q}_h, \hat{\mathbf{q}}_h)) \|_{\bar{\mathbf{X}}_h}^2,
\end{aligned}$$

where $C = \max\{1, \bar{C}_a, 2\bar{C}_b^2\}$. The second estimate follows directly by the definitions of the norms, which yields

$$\begin{aligned} \|(\mathbf{v}_h, \mathbf{q}_h)\|_{\mathbf{Y}_h}^2 &\geq \sum_{i=1}^n R_i \|(q_{i,h}, \hat{q}_{i,h})\|_{\text{HDG}}^2 + \frac{1}{\lambda_0} \left\| \sum_{i=1}^n q_{i,h} \right\|_0^2 + (\Lambda_\zeta \mathbf{q}_h, \mathbf{q}_h) \\ &\quad + \underline{C}_c \|(\mathbf{v}_h, \hat{\mathbf{v}}_h)\|_{\text{HDG}}^2 + \lambda \|\operatorname{div} \mathbf{v}_h\|_0^2 + \sum_{i=1}^n R_i^{-1} \|\mathbf{z}_{i,h}\|_0^2 + |\mathbf{v}_h|_{\mathbf{b}}^2 \\ &\geq C(\|(\mathbf{v}_h, \hat{\mathbf{v}}_h)\|_{\bar{\mathbf{U}}_h}^2 + \|(\mathbf{q}_h, \hat{\mathbf{q}}_h)\|_{\bar{\mathbf{P}}_h}^2 + \|\mathbf{z}_h\|_{\bar{\mathbf{W}}_-}^2) \\ &= C\|((\mathbf{v}_h, \hat{\mathbf{v}}_h), \mathbf{z}_h, (\mathbf{q}_h, \hat{\mathbf{q}}_h))\|_{\bar{\mathbf{X}}_h}^2, \end{aligned}$$

where $C = \min\{1, \underline{C}_c\}$ and \underline{C}_c is the coercivity constant of $a_h^{\text{HDG}}((\cdot, \cdot), (\cdot, \cdot))$. \square

Remark 1. In the case $n = 1$, the definition of norm (16) reduces to the norm (18b) in [17].

5. NUMERICAL EXAMPLES

In this section we demonstrate the applicability of our theoretical results with some numerical experiments. For this, we first propose a norm-equivalent preconditioner following similar steps as in [17]. The preconditioner is then extensively tested with respect to the parameters in several test cases. Finally, we perform some numerical simulations for a 4-network model of a human brain. All numerical experiments are realized in the finite element library Netgen/NGSolve, see [25, 26] and www.ngsolve.org.

5.1. Norm equivalent preconditioners. In [17] the authors already provided a detailed construction of a parameter robust well-posedness theory and preconditioner of the Biot problem, i.e. the case of the MPET problem with $n = 1$. In the following we give a brief overview of the corresponding extension to the MPET problem, but refer to [17] for details regarding implementation aspects and a discussion on using static condensation to eliminate local (element-wise) unknowns from the system. To this end, let $\mathbf{u}_h = ((\mathbf{u}_h, \hat{\mathbf{u}}_h), \mathbf{w}_h)$, $\mathbf{p}_h = (\mathbf{p}_h, \hat{\mathbf{p}}_h)$ be the solution of (19). Using the same notation for the coefficient vectors as for the solutions we can rewrite (19) as

$$(42) \quad \begin{pmatrix} \mathbf{A} & \mathbf{B}^T \\ \mathbf{B} & -\mathbf{C} \end{pmatrix} \begin{pmatrix} \mathbf{u}_h \\ \mathbf{p}_h \end{pmatrix} = \mathbf{F},$$

where $\mathbf{A}, \mathbf{B}, \mathbf{C}$ and \mathbf{F} are the corresponding system matrices and the right hand side vector defined by the bilinear forms (32) and the linear form (33). According to Corollary 5, a norm equivalent preconditioner, compare Section 4.2 in [17], is then given by

$$(43) \quad \mathcal{B} := \begin{pmatrix} \mathbf{X}_{u,w} & \mathbf{0} \\ \mathbf{0} & \mathbf{X}_{p,p} \end{pmatrix},$$

where $\mathbf{X}_{u,w}$ and $\mathbf{X}_{p,p}$ are the system matrices of the bilinear forms induced by the norms used in (18), i.e. $\|\cdot\|_{\bar{\mathbf{U}}_h}^2 + \|\cdot\|_{\bar{\mathbf{W}}_-}^2$ and $\|\cdot\|_{\bar{\mathbf{P}}_h}^2$, respectively. An alternative preconditioner can be proposed following the steps from Section 4.4 in [17]. Since the element-wise block diagonal structure of the part of the matrix \mathbf{A} that corresponds to the bilinear form $\sum_{i=1}^n (R_i^{-1} \mathbf{w}_{i,h}, \mathbf{z}_{i,h})$, see second term in (32a), allows a very efficient inversion, one can eliminate the velocities $\mathbf{w}_{i,h}$ from the system matrix. Then one solves a reduced problem using the stiffness matrix for the displacement (first term in (32a)), the divergence constraints coupling the displacements and the pressures (first term in (32b)), and the resulting pressure Schur complement with respect to the velocities. Using this technique, we introduce the second preconditioner by

$$(44) \quad \tilde{\mathcal{B}} := \begin{pmatrix} \mathbf{X}_u & \mathbf{0} \\ \mathbf{0} & \tilde{\mathbf{X}}_p \end{pmatrix}$$

where \mathbf{X}_u corresponds to the bilinear form induced by the norm $\|\cdot\|_{\tilde{U}_h}^2$ and $\tilde{\mathbf{X}}_p$ is the above mentioned resulting pressure Schur complement. A detailed construction of $\tilde{\mathbf{X}}_p$ is given in equation (63) in [17]. Note that there holds the spectral equivalence $\mathbf{X}_p \approx \tilde{\mathbf{X}}_p$, i.e. both preconditioners \mathcal{B} and $\tilde{\mathcal{B}}$ are well suited to solve the system with an iterative method. However, in accordance with the results from [17], the preconditioner $\tilde{\mathcal{B}}$ performs better, see Section 5.2.1.

5.2. Parameter-robustness. To study the numerical behavior of the norm equivalent preconditioners \mathcal{B} and $\tilde{\mathcal{B}}$ defined in the previous section we consider problem (9) in the 2-network case on the spatial domain $\Omega = (0, 1)^3$ with exact solution

$$\mathbf{u} := (\varphi, \varphi, \varphi), \quad \mathbf{p} := \begin{pmatrix} x^2(1-x)^2y^2(1-y)^2z^2(1-z)^2 \\ \sin(\pi x)^2 \sin(\pi y)^2 \sin(\pi z)^2 \end{pmatrix} - \mathbf{p}_0,$$

where $\varphi = \sin(\pi x) \sin(\pi y) \sin(\pi z)$. The constant vector \mathbf{p}_0 is chosen in such a way that $\mathbf{p} \in L_0^2(\Omega)^2$. We solve the problem using a regular mesh \mathcal{T}_h with varying mesh size. For the interior penalty stabilization parameter η in (7) we choose the value $\eta = 10$. All problems were solved by means of the preconditioned minimal residual method (MinRes) with a fixed tolerance of 10^{-8} . The symmetric positive definite (SPD) preconditioner (in the following section denoted by \mathcal{B} and $\tilde{\mathcal{B}}$) is inverted using a direct method. To simplify the notation we introduce symbols for the (scaled) parameters for the pressures when they coincide, i.e. we have $\alpha_p := \alpha_{p_1} = \alpha_{p_2}$, $R := R_1 = R_2$. If the parameters differ from each other we use the notation used so far. Further note that since we have only two pressures we use the symbol $\xi := \xi_{12} = \xi_{21}$.

5.2.1. Comparison of the preconditioners \mathcal{B} and $\tilde{\mathcal{B}}$. In this first example we want to compare the performance of the MinRes solver using either \mathcal{B} or $\tilde{\mathcal{B}}$ as a preconditioner. To this end, we solve the problem of Section 5.2 using the polynomial order $\ell = 2$, a triangulation with $|\mathcal{T}_h| = 384$ elements, and consider the parameters $\alpha_p = 0, \xi = 0, \lambda = 1$. The value of R is set to 10^{-i} with $i = 0, 2, 4, 6, 8$. Note that the test case of vanishing R and zero values for ξ, α_p is the most challenging one as observed in Section 5.2.2. In Figure 1a and Figure 1b we plot the history of the residual (res) over the number of iterations (it) of the MinRes solver for both preconditioners. Several observations can be made here. First of all note that the plots show a robustness with respect to R since there appears an upper bound of the iterations for $R \rightarrow 0$. To discuss this in more detail we note that (according to [22]) the number of iterations of the MinRes solver particularly depends on the spectral equivalences

$$(45) \quad \mathbf{X}_p \approx \mathbf{S}_p \quad \text{or} \quad \tilde{\mathbf{X}}_p \approx \mathbf{S}_p,$$

when using \mathcal{B} or $\tilde{\mathcal{B}}$, respectively. Here $\mathbf{S}_p := -\mathbf{B}\mathbf{A}^{-1}\mathbf{B}^T - \mathbf{C}$ is the pressure Schur complement (with respect to the displacement \mathbf{u}). Since we have chosen $\alpha_p = \xi = 0$, we see that in the limit $R \rightarrow 0$ the “ \mathbf{C} -block” in the system matrix (42) and in \mathbf{S}_p vanishes. Further, according to definition (16) both matrices \mathbf{X}_p and $\tilde{\mathbf{X}}_p$ then converge to a matrix which is induced by the bilinear form $(\Lambda \mathbf{p}, \mathbf{q})$ which we denote by \mathbf{M}_p^Λ in the following. As we have $\Lambda = \frac{1}{\lambda_0} \mathbb{I}$, see (11), standard estimates (compare [28]) then give the spectral equivalence,

$$(46) \quad \mathbf{B}\mathbf{A}^{-1}\mathbf{B}^T \approx \mathbf{M}_p^\Lambda.$$

This shows that when $R \rightarrow 0$, the spectral equivalences in (45) are dominated by (46) (as \mathbf{C} vanishes), and thus the choice of the elliptic discrete H^1 -part of the pressure preconditioner given by the HDG-norm, see (16), in \mathbf{X}_p , or by the elliptic operator resulting from the elimination of the local velocities (see previous section) in $\tilde{\mathbf{X}}_p$, is not crucial anymore. Summarizing we see that the upper bound of the iterations is independent of the choice of \mathcal{B} and $\tilde{\mathcal{B}}$ and robust in R . However, since the latter version provides better results particularly also for moderate numbers of R , we only consider $\tilde{\mathcal{B}}$ for the rest of this work.

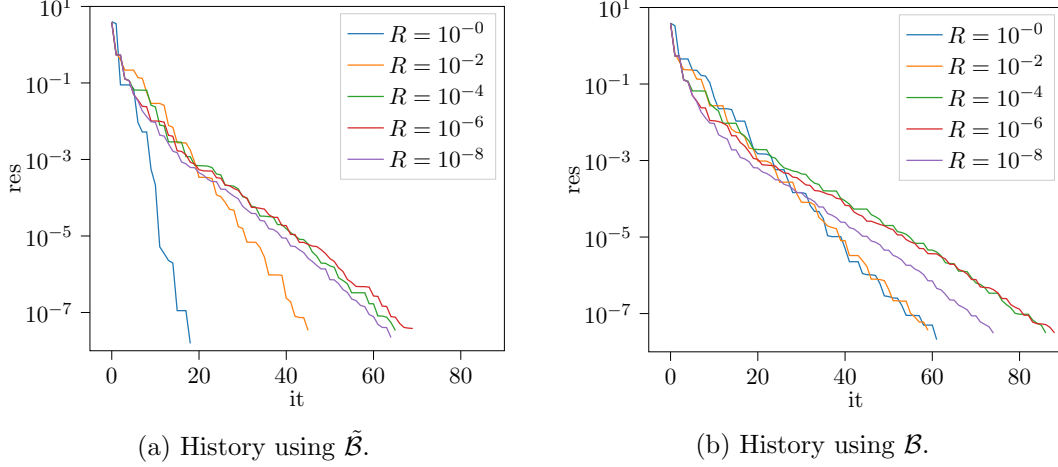


FIGURE 1. History of the residual using the preconditioned Minres solver.

Remark 2. Equations (45) and (46) show why it is essential that $R > 0$. As \mathbf{M}_p^Λ is not SPD the choice $R = 0$ (and $\alpha_p = \xi = 0$) would then lead to non SPD preconditioners \mathbf{X}_p or $\tilde{\mathbf{X}}_p$. In other words the norm in (16) is only a semi norm for $R = \alpha_p = \xi = 0$.

5.2.2. Robustness for equivalent pressure coefficients. We solve the problem of Section 5.2 using the polynomial orders $\ell = 2, 3$ and a fixed mesh with $|\mathcal{T}_h| = 384$ elements. We consider the parameters $\alpha_p = 10^{-i}$, $R = 10^{-i}$, $\xi = 10^{-i}$ with $i = 0, 2, 4, 6, 8$ and $\lambda = 10^j$ with $j = 0, 4, 8$. In Table 1 we have plotted the number of iterations of the MinRes solver in orange color for the polynomial order $\ell = 2$ and in blue color for $\ell = 3$. Although varying slightly, a detailed analysis of the numbers shows a similar behavior as already discussed in the previous section. While being very robust in λ and ξ , smaller values of α_p and R (i.e. the \mathbf{C} -block gets “smaller”, compare discussion below (45)) increase the number of iterations. However, in accordance with the findings from before, an upper bound is given by approximately 70 iterations.

5.2.3. Robustness for different pressure coefficients. Again we solve the problem of Section 5.2 using the polynomial orders $\ell = 2, 3$ and a fixed mesh with $|\mathcal{T}_h| = 384$ elements. In contrast to the previous section we now fix the values of $\alpha_{p_1} = R_1 = 10^{-4}$ and vary $\alpha_{p_2} = 10^{-i}$, $R_2 = 10^{-i}$, $\xi = 10^{-i}$ with $i = 0, 2, 4, 6, 8$ and $\lambda = 10^j$ with $j = 0, 4, 8$. Again, the results of Table 2 show robustness with respect to all parameters. Comparing the results with the numbers from the previous section, see Table 1, we see that for bigger values of α_{p_2} , R_2 the (relatively) smaller parameters α_{p_1} , R_1 slightly increase the number of iterations (the \mathbf{C} -block is “smaller” as before), and for smaller values of α_{p_2} , R_2 the (relatively) larger parameters α_{p_1} , R_1 slightly reduce the number (i.e. the \mathbf{C} -block is “larger” as before).

5.2.4. Robustness with respect to \mathcal{T}_h and the polynomial order ℓ . In the last example we discuss the performance of the preconditioner with respect to the polynomial order and the number of elements of the triangulation. To this end, we solve the problem of Section 5.2 using the polynomial orders $\ell = 1, \dots, 6$ and several meshes with $|\mathcal{T}_h| = 48, 162, 384, 750, 1296, 2058$ elements. We use constant values $\alpha_p = R = \xi = 10^{-4}$ and $\lambda = 1$. Since we have used a direct solver to invert \mathcal{B} and $\tilde{\mathcal{B}}$, a dependency with respect to the mesh size is not expected, and is validated by the numbers of the right Table 3. In addition to that, the results also show that the solver is very robust with respect to the polynomial order.

$\xi = 1$															
$\alpha_p \backslash R^{-1}$	$\lambda = 1$					$\lambda = 1 \cdot 10^4$					$\lambda = 1 \cdot 10^8$				
	1	$1 \cdot 10^2$	$1 \cdot 10^4$	$1 \cdot 10^6$	$1 \cdot 10^8$	1	$1 \cdot 10^2$	$1 \cdot 10^4$	$1 \cdot 10^6$	$1 \cdot 10^8$	1	$1 \cdot 10^2$	$1 \cdot 10^4$	$1 \cdot 10^6$	$1 \cdot 10^8$
1	11,10	22,22	21,21	21,21	21,21	11,10	22,22	21,21	21,21	21,21	11,10	22,22	21,21	21,21	21,21
$1 \cdot 10^{-2}$	11,10	30,30	47,43	53,53	53,53	11,10	30,30	47,43	53,53	53,53	11,10	30,30	47,43	53,53	53,53
$1 \cdot 10^{-4}$	11,10	30,30	48,44	55,56	55,57	11,10	30,30	48,44	55,56	55,57	11,10	30,30	48,44	55,56	55,57
$1 \cdot 10^{-6}$	11,10	30,30	48,44	55,56	55,57	11,10	30,30	48,44	55,56	55,57	11,10	30,30	48,44	55,56	55,57
$1 \cdot 10^{-8}$	11,10	30,30	48,44	55,56	55,57	11,10	30,30	48,44	55,56	55,57	11,10	30,30	48,44	55,56	55,57

$\xi = 1 \cdot 10^{-2}$															
$\alpha_p \backslash R^{-1}$	$\lambda = 1$					$\lambda = 1 \cdot 10^4$					$\lambda = 1 \cdot 10^8$				
	1	$1 \cdot 10^2$	$1 \cdot 10^4$	$1 \cdot 10^6$	$1 \cdot 10^8$	1	$1 \cdot 10^2$	$1 \cdot 10^4$	$1 \cdot 10^6$	$1 \cdot 10^8$	1	$1 \cdot 10^2$	$1 \cdot 10^4$	$1 \cdot 10^6$	$1 \cdot 10^8$
1	11,10	22,22	21,21	21,21	21,21	11,10	22,22	21,21	21,21	21,21	11,10	22,22	21,21	21,21	21,21
$1 \cdot 10^{-2}$	13,12	30,30	48,44	54,54	53,53	13,12	30,30	48,44	54,54	53,53	13,12	30,30	48,44	54,54	53,53
$1 \cdot 10^{-4}$	13,12	30,30	48,44	56,56	55,57	13,12	30,30	48,44	56,56	55,57	13,12	30,30	48,44	56,56	55,57
$1 \cdot 10^{-6}$	13,12	30,30	48,44	56,56	55,57	13,12	30,30	48,44	56,56	55,57	13,12	30,30	48,44	56,56	55,57
$1 \cdot 10^{-8}$	13,12	30,30	48,44	56,56	55,57	13,12	30,30	48,44	56,56	55,57	13,12	30,30	48,44	56,56	55,57

$\xi = 1 \cdot 10^{-4}$															
$\alpha_p \backslash R^{-1}$	$\lambda = 1$					$\lambda = 1 \cdot 10^4$					$\lambda = 1 \cdot 10^8$				
	1	$1 \cdot 10^2$	$1 \cdot 10^4$	$1 \cdot 10^6$	$1 \cdot 10^8$	1	$1 \cdot 10^2$	$1 \cdot 10^4$	$1 \cdot 10^6$	$1 \cdot 10^8$	1	$1 \cdot 10^2$	$1 \cdot 10^4$	$1 \cdot 10^6$	$1 \cdot 10^8$
1	11,10	22,22	21,21	21,21	21,21	11,10	22,22	21,21	21,21	21,21	11,10	22,22	21,21	21,21	21,21
$1 \cdot 10^{-2}$	13,12	30,30	48,44	54,54	53,53	13,12	30,30	48,44	54,54	53,53	13,12	30,30	48,44	54,54	53,53
$1 \cdot 10^{-4}$	13,12	34,34	48,45	57,58	56,58	13,12	34,34	48,45	57,58	56,58	13,12	34,34	48,45	57,58	56,58
$1 \cdot 10^{-6}$	15,12	34,34	48,45	57,58	56,58	15,12	34,34	48,45	57,58	56,58	15,12	34,34	48,45	57,58	56,58
$1 \cdot 10^{-8}$	13,14	34,34	48,45	57,58	56,58	13,14	34,34	48,45	57,58	56,58	13,14	34,34	48,45	57,58	56,58

$\xi = 1 \cdot 10^{-6}$															
$\alpha_p \backslash R^{-1}$	$\lambda = 1$					$\lambda = 1 \cdot 10^4$					$\lambda = 1 \cdot 10^8$				
	1	$1 \cdot 10^2$	$1 \cdot 10^4$	$1 \cdot 10^6$	$1 \cdot 10^8$	1	$1 \cdot 10^2$	$1 \cdot 10^4$	$1 \cdot 10^6$	$1 \cdot 10^8$	1	$1 \cdot 10^2$	$1 \cdot 10^4$	$1 \cdot 10^6$	$1 \cdot 10^8$
1	11,10	22,22	21,21	21,21	21,21	11,10	22,22	21,21	21,21	21,21	11,10	22,22	21,21	21,21	21,21
$1 \cdot 10^{-2}$	13,12	31,30	48,44	54,54	53,53	13,12	31,30	48,44	54,54	53,53	13,12	31,30	48,44	54,54	53,53
$1 \cdot 10^{-4}$	15,14	35,36	49,45	57,58	56,58	15,14	35,36	49,45	57,58	56,58	15,14	35,36	49,45	57,58	56,58
$1 \cdot 10^{-6}$	15,14	39,38	54,50	61,63	59,59	15,14	39,38	54,50	61,63	59,59	15,14	39,38	54,50	61,63	59,59
$1 \cdot 10^{-8}$	15,14	40,40	56,51	61,62	59,59	15,14	40,40	56,51	61,62	59,59	15,14	40,40	56,51	61,62	59,59

$\xi = 1 \cdot 10^{-8}$															
$\alpha_p \backslash R^{-1}$	$\lambda = 1$					$\lambda = 1 \cdot 10^4$					$\lambda = 1 \cdot 10^8$				
	1	$1 \cdot 10^2$	$1 \cdot 10^4$	$1 \cdot 10^6$	$1 \cdot 10^8$	1	$1 \cdot 10^2$	$1 \cdot 10^4$	$1 \cdot 10^6$	$1 \cdot 10^8$	1	$1 \cdot 10^2$	$1 \cdot 10^4$	$1 \cdot 10^6$	$1 \cdot 10^8$
1	11,10	22,22	21,21	21,21	21,21	11,10	22,22	21,21	21,21	21,21	11,10	22,22	21,21	21,21	21,21
$1 \cdot 10^{-2}$	13,12	31,30	48,44	54,54	53,53	13,12	31,30	48,44	54,54	53,53	13,12	31,30	48,44	54,54	53,53
$1 \cdot 10^{-4}$	15,14	36,34	49,45	57,58	56,58	15,14	36,34	49,45	57,58	56,58	15,14	36,34	49,45	57,58	56,58
$1 \cdot 10^{-6}$	17,14	40,40	56,52	61,61	59,59	17,14	40,40	56,52	61,61	59,59	17,14	40,40	56,52	61,61	59,59
$1 \cdot 10^{-8}$	19,16	44,45	63,58	66,67	63,64	19,16	44,45	63,58	66,67	63,64	19,16	44,45	63,58	66,67	63,64

TABLE 1. Results for the first test case of Section 5.2.2. Orange color is used for $\ell = 2$, blue for $\ell = 3$.

$\xi = 1$															
$\alpha_{p_2} \backslash R_2^{-1}$	$\lambda = 1$					$\lambda = 1 \cdot 10^4$					$\lambda = 1 \cdot 10^8$				
	1	$1 \cdot 10^2$	$1 \cdot 10^4$	$1 \cdot 10^6$	$1 \cdot 10^8$	1	$1 \cdot 10^2$	$1 \cdot 10^4$	$1 \cdot 10^6$	$1 \cdot 10^8$	1	$1 \cdot 10^2$	$1 \cdot 10^4$	$1 \cdot 10^6$	$1 \cdot 10^8$
1	18,18	25,26	27,27	27,27	27,27	18,18	25,26	27,27	27,27	27,27	18,18	25,26	27,27	27,27	27,27
$1 \cdot 10^{-2}$	18,18	31,31	47,43	50,47	50,47	18,18	31,31	47,43	50,47	50,47	18,18	31,31	47,43	50,47	50,47
$1 \cdot 10^{-4}$	18,18	31,31	48,44	51,48	51,48	18,18	31,31	48,44	51,48	51,48	18,18	31,31	48,44	51,48	51,48
$1 \cdot 10^{-6}$	18,18	31,31	48,44	51,48	51,48	18,18	31,31	48,44	51,48	51,48	18,18	31,31	48,44	51,48	51,48
$1 \cdot 10^{-8}$	18,18	31,31	48,44	51,48	51,48	18,18	31,31	48,44	51,48	51,48	18,18	31,31	48,44	51,48	51,48

$\xi = 1 \cdot 10^{-2}$															
$\alpha_{p_2} \backslash R_2^{-1}$	$\lambda = 1$					$\lambda = 1 \cdot 10^4$					$\lambda = 1 \cdot 10^8$				
	1	$1 \cdot 10^2$	$1 \cdot 10^4$	$1 \cdot 10^6$	$1 \cdot 10^8$	1	$1 \cdot 10^2$	$1 \cdot 10^4$	$1 \cdot 10^6$	$1 \cdot 10^8$	1	$1 \cdot 10^2$	$1 \cdot 10^4$	$1 \cdot 10^6$	$1 \cdot 10^8$
1	42,41	43,41	43,40	43,39	43,39	42,41	43,41	43,40	43,39	43,39	42,41	43,41	43,40	43,39	43,39
$1 \cdot 10^{-2}$	46,45	44,41	48,44	52,52	52,52	46,45	44,41	48,44	52,52	52,52	46,45	44,41	48,44	52,52	52,52
$1 \cdot 10^{-4}$	47,45	44,41	48,44	54,54	54,54	47,45	44,41	48,44	54,54	54,54	47,45	44,41	48,44	54,54	54,54
$1 \cdot 10^{-6}$	47,45	44,41	48,44	54,54	54,54	47,45	44,41	48,44	54,54	54,54	47,45	44,41	48,44	54,54	54,54
$1 \cdot 10^{-8}$	46,45	44,41	48,44	54,54	54,54	46,45	44,41	48,44	54,54	54,54	46,45	44,41	48,44	54,54	54,54

$\xi = 1 \cdot 10^{-4}$															
$\alpha_{p_2} \backslash R_2^{-1}$	$\lambda = 1$					$\lambda = 1 \cdot 10^4$					$\lambda = 1 \cdot 10^8$				
	1	$1 \cdot 10^2$	$1 \cdot 10^4$	$1 \cdot 10^6$	$1 \cdot 10^8$	1	$1 \cdot 10^2$	$1 \cdot 10^4$	$1 \cdot 10^6$	$1 \cdot 10^8$	1	$1 \cdot 10^2$	$1 \cdot 10^4$	$1 \cdot 10^6$	$1 \cdot 10^8$
1	45,41	44,41	45,40	45,40	45,40	45,41	44,41	45,40	45,40	45,40	45,41	44,41	45,40	45,40	45,40
$1 \cdot 10^{-2}$	51,48	46,41	48,45	53,52	54,52	51,48	46,41	48,45	53,52	54,52	51,48	46,41	48,45	53,52	54,52
$1 \cdot 10^{-4}$	55,52	49,46	48,45	57,59	57,59	55,52	49,46	48,45	57,59	57,59	55,52	49,46	48,45	57,59	57,59
$1 \cdot 10^{-6}$	57,52	49,46	48,45	57,59	59,58	57,52	49,46	48,45	57,59	59,58	57,52	49,46	48,45	57,59	59,58
$1 \cdot 10^{-8}$	55,52	49,46	48,45	57,59	57,59	55,52	49,46	48,45	57,59	57,59	55,52	49,46	48,45	57,59	57,59

$\xi = 1 \cdot 10^{-6}$															
$\alpha_{p_2} \backslash R_2^{-1}$	$\lambda = 1$					$\lambda = 1 \cdot 10^4$					$\lambda = 1 \cdot 10^8$				
	1	$1 \cdot 10^2$	$1 \cdot 10^4$	$1 \cdot 10^6$	$1 \cdot 10^8$	1	$1 \cdot 10^2$	$1 \cdot 10^4$	$1 \cdot 10^6$	$1 \cdot 10^8$	1	$1 \cdot 10^2$	$1 \cdot 10^4$	$1 \cdot 10^6$	$1 \cdot 10^8$
1	46,41	44,41	45,40	45,40	45,40	46,41	44,41	45,40	45,40	45,40	46,41	44,41	45,40	45,40	45,40
$1 \cdot 10^{-2}$	51,48	47,41	48,45	53,52	54,53	51,48	47,41	48,45	53,52	54,53	51,48	47,41	48,45	53,52	54,53
$1 \cdot 10^{-4}$	57,54	51,47	49,45	60,60	60,62	57,54	51,47	49,45	60,60	60,62	57,54	51,47	49,45	60,60	60,62
$1 \cdot 10^{-6}$	58,55	52,49	49,46	60,60	60,61	58,55	52,49	49,46	60,60	60,61	58,55	52,49	49,46	60,60	60,61
$1 \cdot 10^{-8}$	59,56	52,49	49,46	60,60	60,61	59,56	52,49	49,46	60,60	60,61	59,56	52,49	49,46	60,60	60,61

$\xi = 1 \cdot 10^{-8}$															
$\alpha_{p_2} \backslash R_2^{-1}$	$\lambda = 1$					$\lambda = 1 \cdot 10^4$					$\lambda = 1 \cdot 10^8$				
	1	$1 \cdot 10^2$	$1 \cdot 10^4$	$1 \cdot 10^6$	$1 \cdot 10^8$	1	$1 \cdot 10^2$	$1 \cdot 10^4$	$1 \cdot 10^6$	$1 \cdot 10^8$	1	$1 \cdot 10^2$	$1 \cdot 10^4$	$1 \cdot 10^6$	$1 \cdot 10^8$
1	46,41	44,41	45,40	45,40	45,40	46,41	44,41	45,40	45,40	45,40	46,41	44,41	45,40	45,40	45,40
$1 \cdot 10^{-2}$	51,48	46,41	48,45	53,52	54,53	51,48	46,41	48,45	53,52	54,53	51,48	46,41	48,45	53,52	54,53
$1 \cdot 10^{-4}$	58,54	51,47	49,45	60,60	60,62	58,54	51,47	49,45	60,60	60,62	58,54	51,47	49,45	60,60	60,62
$1 \cdot 10^{-6}$	59,56	52,49	49,46	60,60	60,61	59,56	52,49	49,46	60,60	60,61	59,56	52,49	49,46	60,60	60,61
$1 \cdot 10^{-8}$	58,56	52,49	49,46	60,60	60,61	58,56	52,49	49,46	60,60	60,61	58,56	52,49	49,46	60,60	60,61

TABLE 2. Results for the second test case of Section 5.2.3. Orange color is used for $\ell = 2$, blue for $\ell = 3$.

$\ell \backslash \mathcal{T}_h $	48	162	384	750	1296	2058
1	19	37	50	53	53	52
2	46	52	48	46	44	44
3	50	48	45	43	41	41
4	52	49	46	43	41	41
5	51	46	43	41	41	41
6	47	43	42	41	42	42

TABLE 3. Results for the third test case of Section 5.2.4.

5.3. Four-network model of the human brain. As an application of the MPET formulation (1), we consider a 4-network model of the human brain. This model has already been studied for the total pressure formulation, e.g. in [20]. The brain geometry Ω originates from the Colin 27 Adult Brain Atlas FEM mesh. The surface $\partial\Omega$ is split into the outer boundary representing the skull Γ_s , and the inner boundary representing the ventricles Γ_v . For the computations we use the same mesh as in [20, 23] with 99605 elements and 29037 vertices, see Figure 2a. We take for the unscaled parameters in problem (1) the values summarized in Table 4. Note that the Lamé parameters can be expressed in terms of Young's modulus of elasticity E and the Poisson ratio $\nu \in [0, 1/2)$ via $\lambda = \frac{\nu E}{(1+\nu)(1-2\nu)}$, and $\mu = \frac{E}{2(1+\nu)}$. For the boundary conditions (all values given in mmHg) we use

$$\begin{aligned}
p_1 &= 5 + 2 \sin(2\pi t) & \text{on } \Gamma_s, & & p_1 &= 5 + 2.012 \sin(2\pi t) & \text{on } \Gamma_v, \\
p_2 &= 70 + 10 \sin(2\pi t) & \text{on } \Gamma_s, & & \nabla p_2 \cdot \mathbf{n} &= 0 & \text{on } \Gamma_v, \\
p_3 &= 6 & \text{on } \Gamma_s, & & p_3 &= 6 & \text{on } \Gamma_v, \\
\nabla p_4 \cdot \mathbf{n} &= 0 & \text{on } \Gamma_s, & & \nabla p_4 \cdot \mathbf{n} &= 0 & \text{on } \Gamma_v, \\
\mathbf{u} &= 0 & \text{on } \Gamma_s, & & \boldsymbol{\sigma} \mathbf{n} &= - \sum_{i=1}^4 \alpha_i p_{i,V} \mathbf{n} & \text{on } \Gamma_v,
\end{aligned}$$

where $p_{i,V}$ for $i = 1, \dots, 4$ are prescribed pressures on the ventricles given by

$$p_{1,V} = 5 + 2.012 \sin(2\pi t), \quad p_{2,V} = 70 + 10 \sin(2\pi t), \quad p_{3,V} = 6, \quad p_{4,V} = 38.$$

The initial conditions from [20] for $t = 0$ are given by $\mathbf{u} = 0, p_1 = 5, p_2 = 70, p_3 = 6$, and $p_4 = 38$. We solved the time dependent problem using different timesteps (discussed in detail below) and a fixed polynomial order of $\ell = 1$. For each timestep the problem was solved iteratively converging with approximately 15 iterations.

As a first test and to compare our results with [20] we used a timestep size of $\tau = 0.0125s$ and solved the problem until $T = 3$. In Figure 2 we can see the absolute value of the displacement and the pressure distributions at $t = 0.25s$. Further we plotted in Figure 3 and Figure 4 the absolute value of the displacement and the pressures at three fixed points in space given by $P_1 = (89.9, 108.9, 82.3)$, $P_2 = (102.2, 139.3, 82.3)$, and $P_3 = (110.7, 108.9, 98.5)$, which are located close to the ventricles. We see that the results are in agreement with [20]. The biggest difference appears in the extra-cellular pressure p_1 which in our simulations does not exhibit the oscillating behavior that can be found in [20]. To discuss this in more detail let us recall the unscaled equations (1b)–(1c) for $i = 1$

$$(47) \quad \frac{\partial}{\partial t} s_1 p_1 - \operatorname{div}(K_1 \nabla p_1) + (\xi_{12} + \xi_{13} + \xi_{14}) p_1 = \tilde{g}_i - \frac{\partial}{\partial t} \alpha_i \operatorname{div} \mathbf{u} + \xi_{12} p_2 + \xi_{13} p_3 + \xi_{14} p_4,$$

with (see Table 4)

$$s_1 = 3.9 \cdot 10^{-4} \quad \text{and} \quad K_1 = 1.57 \cdot 10^{-5} \quad \text{and} \quad \xi_1 := \xi_{12} + \xi_{13} + \xi_{14} = 2 \cdot 10^{-6}.$$

This shows that if p_1 is stationary ($\partial p_1 / \partial t = 0$) the magnitude of the diffusive coefficient K_1 is bigger as the source coefficient ξ_1 , i.e. no boundary layer is expected. However if the time

derivative dominates (in addition to s_1 being ten times bigger as K_1) a boundary layer might occur in certain cases depending on the right hand side and the considered boundary conditions. Although our triangulation does not inherit a boundary refinement which would be needed to surpass oscillations appearing from non resolved boundary layers when using continuous finite elements, our discretization (19) is not effected by non physical oscillations since boundary conditions are only incorporated in a weak (Nitsche-like) sense. Indeed, the evaluation of the extra-cellular pressure p_1 in Figure 2c appears to be nearly constant. In contrast to p_1 all other pressures do not show a boundary layer which can be explained by the much bigger diffusive coefficients K_2, K_3 and K_4 (compared to corresponding coefficients s_i).

Since the pressures p_1 and p_2 in Figure 4a and Figure 4d suggest that the system is not in a steady periodic state yet, we calculated a long term simulation until $T = 2500s$ with a time step $\tau = 0.125s$. In Figure 5 we have plotted the periodic mean values of the pressures at the points P_j defined by

$$\langle p_i \rangle(P_j, t_k) := \int_{t_k-1/2}^{t_k+1/2} p_i(P_j, s) ds,$$

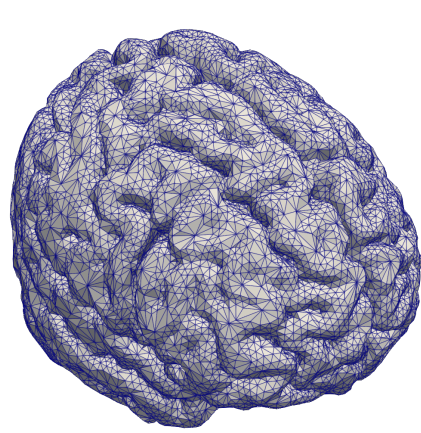
and a periodic solution appears at approximately $t = 1500s$. The definition of the mean value $\langle \cdot \rangle(\cdot, t_k)$ was appropriately changed for $t_k < 0.5$. Note that although Figure 5c suggests a non-smooth time dependency of the venous pressure at the beginning, Figure 4c reveals that there is a steep but smooth increase.

parameter	value	unit
ν	0.4999	
E	1500	Nm ⁻²
s_1	$3.9 * 10^{-4}$	N ⁻¹ m ²
$s_2 = s_4$	$2.9 * 10^{-4}$	N ⁻¹ m ²
s_3	$1.5 * 10^{-5}$	N ⁻¹ m ²
α_1	0.49	
$\alpha_2 = \alpha_4$	0.25	
α_3	0.01	
K_1	$1.57 * 10^{-5}$	mm ² N ⁻¹ m ² s ⁻¹
$K_2 = K_3 = K_4$	$3.75 * 10^{-2}$	mm ² N ⁻¹ m ² s ⁻¹
$\xi_{13} = \xi_{14}$	$1.0 * 10^{-6}$	N ⁻¹ m ² s ⁻¹
$\xi_{24} = \xi_{34}$	$1.0 * 10^{-6}$	N ⁻¹ m ² s ⁻¹
$\xi_{12} = \xi_{23}$	0.0	N ⁻¹ m ² s ⁻¹

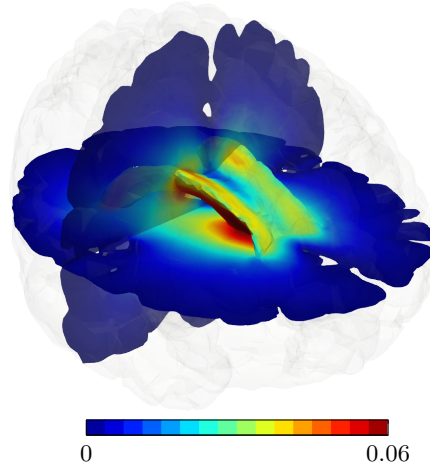
TABLE 4. Reference values of model parameters for the four-network brain model taken from [20].

REFERENCES

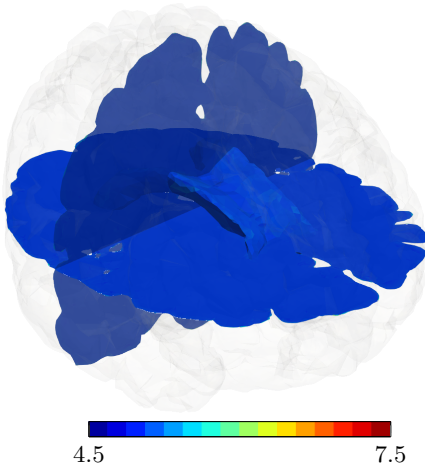
- [1] Douglas N Arnold, Franco Brezzi, Bernardo Cockburn, and L Donatella Marini. Unified analysis of discontinuous Galerkin methods for elliptic problems. *SIAM journal on numerical analysis*, 39(5):1749–1779, 2002.
- [2] D. Boffi, F. Brezzi, and M. Fortin. *Mixed finite element methods and applications*, volume 44 of *Springer Ser. Comput. Math.* Springer, Heidelberg, 2013.
- [3] Dean Chou, John C. Vardakis, Liwei Guo, Brett J. Tully, and Yiannis Ventikos. A fully dynamic multi-compartmental poroelastic system: Application to aqueductal stenosis. *Journal of Biomechanics*, 49(11):2306–2312, 2016. Selected Articles from the International Conference on CFD in Medicine and Biology (Albufeira, Portugal – August 30th - September 4th, 2015).
- [4] Bernardo Cockburn and Jayadeep Gopalakrishnan. A characterization of hybridized mixed methods for second order elliptic problems. *SIAM J. Numer. Anal.*, 42(1):283–301, 2004.



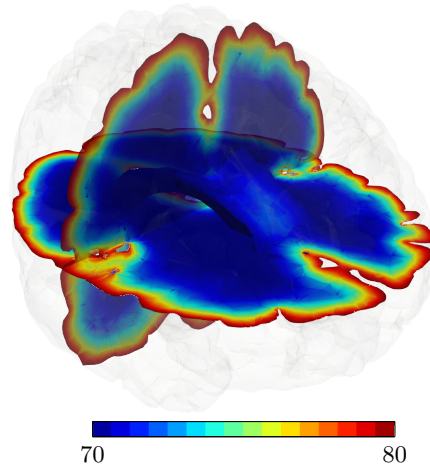
(a) Triangulation



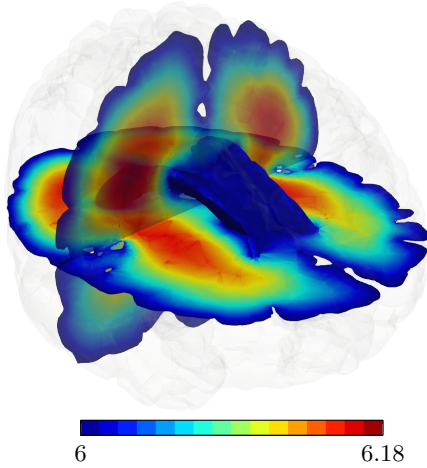
(b) Absolute value of displacement (mm)



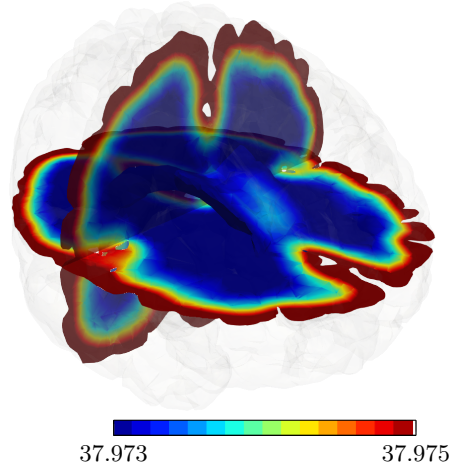
(c) Extra-cellular pressure (mmHg)



(d) Arterial pressure (mmHg)

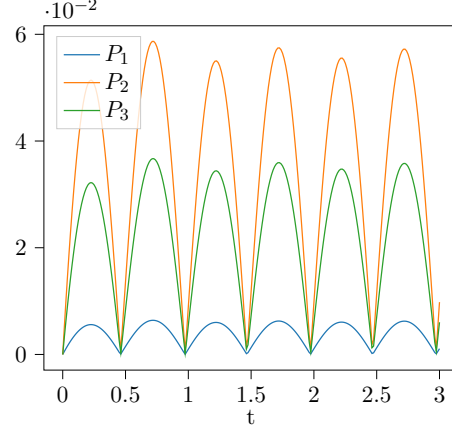
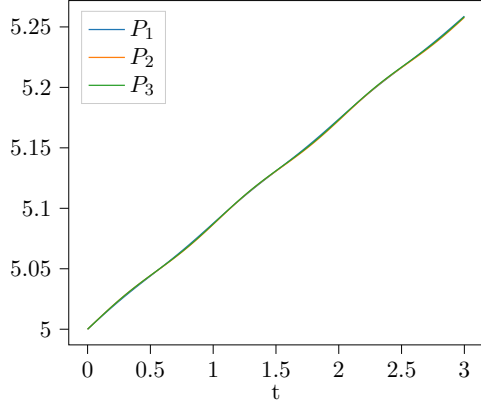


(e) Venous pressure (mmHg)

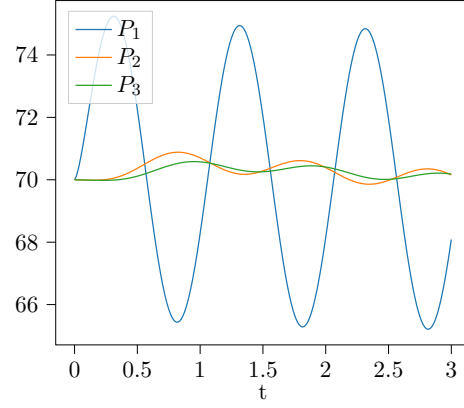


(f) Capillary pressure (mmHg)

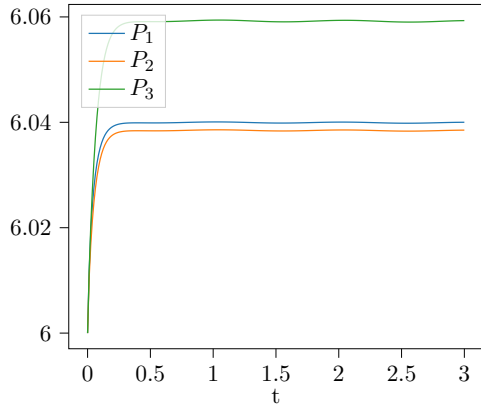
FIGURE 2. Triangulation of the human brain and the absolute value of the displacement and pressure distributions for $t = 0.25$.

FIGURE 3. Evaluation of $|u|$ at P_1 , P_2 and P_3 (mm).

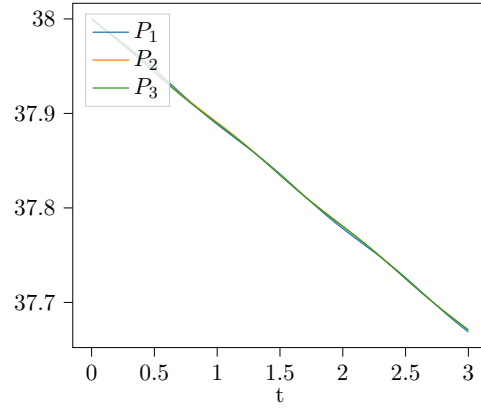
(a) Evaluation of the extra-cellular pressure



(b) Evaluation of the arterial pressure



(c) Evaluation of the venous pressure



(d) Evaluation of the capillary pressure

FIGURE 4. Evaluation of p_1, p_2, p_3, p_4 at P_1 , P_2 and P_3 (mmHg).

- [5] Bernardo Cockburn and Jayadeep Gopalakrishnan. Incompressible finite elements via hybridization. part i: The stokes system in two space dimensions. *SIAM Journal on Numerical Analysis*, 43(4):1627–1650, 2005.
- [6] Bernardo Cockburn and Jayadeep Gopalakrishnan. Incompressible finite elements via hybridization. part ii: The stokes system in three space dimensions. *SIAM Journal on Numerical Analysis*, 43(4):1651–1672, 2005.

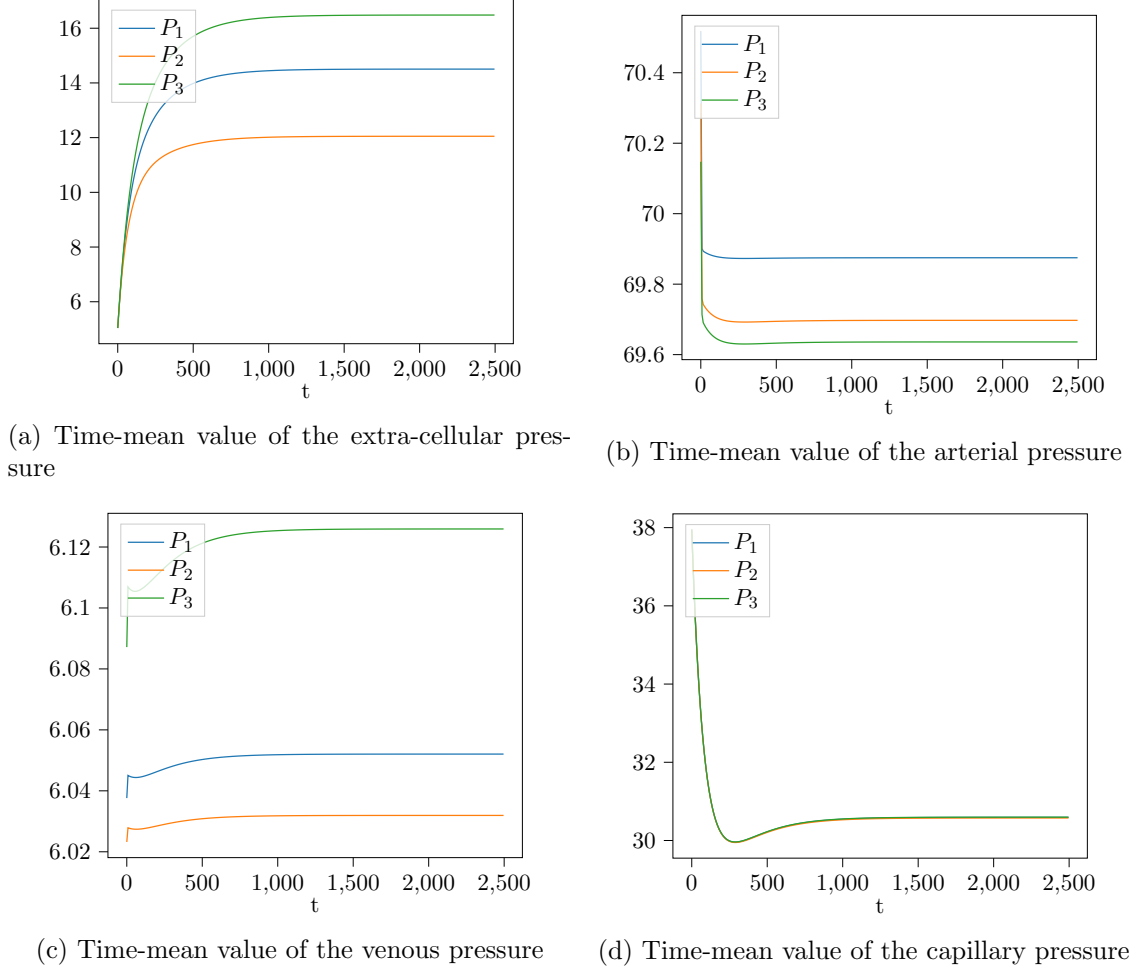


FIGURE 5. Evaluation of the mean values $\langle p_1 \rangle, \langle p_2 \rangle, \langle p_3 \rangle, \langle p_4 \rangle$ at P_1 , P_2 and P_3 (mmHg).

- [7] Bernardo Cockburn, Jayadeep Gopalakrishnan, and Raytcho Lazarov. Unified hybridization of discontinuous Galerkin, mixed, and continuous Galerkin methods for second order elliptic problems. *SIAM J. Numer. Anal.*, 47(2):1319–1365, 2009.
- [8] Bernardo Cockburn, Guido Kanschat, and Dominik Schötzau. A locally conservative LDG method for the incompressible Navier-Stokes equations. *Math. Comp.*, 74(251):1067–1095, 2005.
- [9] Bernardo Cockburn, Guido Kanschat, Dominik Schötzau, and Christoph Schwab. Local discontinuous Galerkin methods for the Stokes system. *SIAM J. Numer. Anal.*, 40(1):319–343, 2002.
- [10] Stefania Fresca and Andrea Manzoni. Real-time simulation of parameter-dependent fluid flows through deep learning-based reduced order models. *Fluids*, 6(7), 2021.
- [11] Liwei Guo, John Vardakis, Toni Lassila, Micaela Mitolo, Nishant Ravikumar, Dean Chou, Matthias Lange, Ali Sarraami-Foroushani, Brett Tully, Zeike Taylor, Susheel Varma, Annalena Venneri, Alejandro Frangi, and Yiannis Ventikos. Subject-specific multiporoelastic model for exploring the risk factors associated with the early stages of alzheimer’s disease. *Interface Focus*, 8, 12 2017.
- [12] Liwei Guo, John C. Vardakis, Dean Chou, and Yiannis Ventikos. A multiple-network poroelastic model for biological systems and application to subject-specific modelling of cerebral fluid transport. *International Journal of Engineering Science*, 147:103204, 2020.
- [13] Q. Hong, J. Kraus, M. Lymbery, and F. Philo. Conservative discretizations and parameter-robust preconditioners for Biot and multiple-network flux-based poroelasticity models. *Numer. Linear Algebra Appl.*, 2019. e2242.
- [14] Q. Hong, J. Kraus, M. Lymbery, and F. Philo. A new framework for the stability analysis of perturbed saddle-point problems and applications in poromechanics. *arXiv:2103.09357v3 [math.NA]*, 2021.

- [15] Qingguo Hong and Johannes Kraus. Parameter-robust stability of classical three-field formulation of Biot’s consolidation model. *ETNA - Electronic Transactions on Numerical Analysis*, 48:202–226, 2018.
- [16] Justin A. Kauffman, Jason P. Sheldon, and Scott T. Miller. Overset meshing coupled with hybridizable discontinuous galerkin finite elements. *International Journal for Numerical Methods in Engineering*, 112(5), 3 2017.
- [17] Johannes Kraus, Philip L. Lederer, Maria Lymbery, and Joachim Schöberl. Uniformly well-posed hybridized discontinuous Galerkin/hybrid mixed discretizations for Biot’s consolidation model. *Computer Methods in Applied Mechanics and Engineering*, 384:113991, 2021.
- [18] Philip L. Lederer, Christoph Lehrenfeld, and Joachim Schöberl. Hybrid discontinuous Galerkin methods with relaxed $H(\text{div})$ -conformity for incompressible flows. Part I. *SIAM J. Numer. Anal.*, 56(4):2070–2094, 2018.
- [19] Philip L. Lederer, Christoph Lehrenfeld, and Joachim Schöberl. Hybrid discontinuous Galerkin methods with relaxed $H(\text{div})$ -conformity for incompressible flows. Part II. *ESAIM Math. Model. Numer. Anal.*, 53(2):503–522, 2019.
- [20] J. Lee, E. Piersanti, K.-A. Mardal, and M. Rognes. A mixed finite element method for nearly incompressible multiple-network poroelasticity. *SIAM J. Sci. Comput.*, 41:A722–A747, 2019.
- [21] Christoph Lehrenfeld and Joachim Schöberl. High order exactly divergence-free hybrid discontinuous Galerkin methods for unsteady incompressible flows. *Comput. Methods Appl. Mech. Engrg.*, 307:339–361, 2016.
- [22] D. Loghin and A. J. Wathen. Analysis of preconditioners for saddle-point problems. *SIAM J. Sci. Comput.*, 25(6):2029–2049, 2004.
- [23] E. Piersanti and M. E. Rognes. Supplementary material (code) for A mixed finite element method for nearly incompressible multiple- network poroelasticity’ by J. J. Lee, E. Piersanti, K.-A. Mardal and M. E. Rognes., April 2018.
- [24] Population Division of the United Nations Department of Economic and Social Affairs (UN DESA). World population ageing 2020 highlights. https://www.un.org/development/desa/pd/sites/www.un.org.development.desa.pd/files/files/documents/2020/Sep/un_pop_2020_pf_ageing_10_key_messages.pdf, 2020.
- [25] J. Schöberl. NETGEN An advancing front 2D/3D-mesh generator based on abstract rules. *Computing and Visualization in Science*, 1(1):41–52, 1997.
- [26] J. Schöberl. C++11 Implementation of Finite Elements in NGSolve. *Institute for Analysis and Scientific Computing, Vienna University of Technology*, 2014.
- [27] John C. Vardakis, Dean Chou, Brett J. Tully, Chang C. Hung, Tsong H. Lee, Po-Hsiang Tsui, and Yiannis Ventikos. Investigating cerebral oedema using poroelasticity. *Medical Engineering & Physics*, 38(1):48–57, 2016. Micro and Nano Flows 2014 (MNF2014) - Biomedical Stream.
- [28] R. Verfürth. A combined conjugate gradient-multigrid algorithm for the numerical solution of the Stokes problem. *IMA J. Numer. Anal.*, 4(4):441–455, 1984.

FACULTY OF MATHEMATICS, UNIVERSITY DUISBURG-ESSEN, GERMANY

Email address: johannes.kraus@uni-due.de

DEPARTMENT OF MATHEMATICS AND SYSTEMS ANALYSIS, AALTO UNIVERSITY, FINLAND

Email address: philip.lederer@aalto.fi

FACULTY OF MATHEMATICS, UNIVERSITY DUISBURG-ESSEN, GERMANY

Email address: maria.lymbery@uni-due.de

FACULTY OF MATHEMATICS, UNIVERSITY DUISBURG-ESSEN, GERMANY

Email address: kevin.osthues@uni-due.de

INSTITUTE FOR ANALYSIS AND SCIENTIFIC COMPUTING, TU WIEN, AUSTRIA

Email address: joachim.schoeberl@tuwien.ac.at